

# Quantum Circuit Compiler for a Shuttling-Based Trapped-Ion Quantum Computer

Fabian Kreppel<sup>1</sup>, Christian Melzer<sup>2</sup>, Janis Wagner<sup>2</sup>, Janine Hilder<sup>2</sup>, Ulrich Poschinger<sup>2</sup>, Ferdinand Schmidt-Kaler<sup>2</sup>, and André Brinkmann<sup>1</sup>

<sup>1</sup>Institute of Computer Science, Johannes Gutenberg University, Anselm-Franz-von-Bentzel-Weg 12, 55128 Mainz, Germany

<sup>2</sup>Institute of Physics, Johannes Gutenberg University, Staudingerweg 7, 55128 Mainz, Germany

Increasing capabilities of quantum computing hardware and the challenge to realize deep quantum circuits call for fully automated and efficient tools to compile quantum circuits. To express arbitrary circuits in a sequence of native gates pertaining to the specific quantum computer architecture is necessary to make algorithms portable across the landscape of quantum hardware providers. In this work, we present a compiler capable of transforming and optimizing a quantum circuit, targeting a shuttling-based trapped-ion quantum processor. It consists of custom algorithms set on top of the Cambridge Quantum Computer’s quantum circuit framework Pytket. The performance is evaluated for a wide range of quantum circuits, showing that the gate counts can be reduced by a factor of up to 3.6 compared to standard Pytket and up to 2.2 compared to standard Qiskit compilation, while we achieve similar gate counts as compared to a Pytket extension targeting the AQT linear-static trapped ion addressing-based architecture.

## 1 Introduction

The current rapid maturation of quantum information processing platforms [1] renders meaningful scientific and commercial applications of quantum computers to be within reach. While it seems unlikely that fault-tolerant devices [2, 3] will scale to sufficiently large logical qubit numbers in the near future, noisy intermediate-scale (NISQ) quantum devices are predicted to usher in the era of applied quantum computing [4]. The capabilities and performance of such platforms will be crucially determined by their quantum compiler stack: First, fully automated, hard-

ware agnostic frontends enable access for non-expert users from various scientific disciplines and industry. Second, optimizations carried out at the compilation stage allow for circumventing limitations due to noise and limited qubit register sizes, thereby enabling increased functionality of a given NISQ platform.

With the scaling up of quantum hardware to larger qubit register sizes and deeper gate sequences, the platforms become increasingly complex and require tool support and automation. Thus, it is no longer feasible to manually design quantum circuits and use fixed decomposition schemes to convert the algorithm input into a complete set of qubit operations which can be executed by the specific quantum hardware, referred to as its *native gate set*. Dedicated quantum compilers are required for the optimized conversion of large circuits to low-level hardware instructions.

In this work, we present such a circuit compiler developed for a shuttling-based trapped-ion quantum computer platform [5, 6, 7]. This platform employs qubits encoded in long-lived states of atomic ions, stored in segmented microchip ion traps as depicted in Fig. 1. In order to increase potential scalability, subsets of the register are stored at different trap sites, and the register is dynamically reconfigured between subsequent gate operations by shuttling operations, which are carried out by controllably changing voltages applied to the trap electrodes. Gates are performed at specific trap sites and are driven by laser or microwave radiation. While this approach enables effective all-to-all connectivity within the register and avoids cross-talk errors [8], the shuttling operations incur substantial timing overhead, leading to rather slow operation timescales. This can lead to increased error rates, as dephasing is aggravated by the reduced operation speed. Furthermore, the shuttling operations can lead to reduced gate fidelities via shuttling-induced heating of the qubit ions. Therefore, besides compiling a given circuit to a native gate set, the main task of the gate compiler stage of a shuttling-based platform is to condition the circuit such that the required amount of shuttling operations can be minimized. This is accomplished by minimizing the overall gate count and by arranging the execution order of the gates in a favourable way. The task of gener-

Fabian Kreppel: [f.kreppel@uni-mainz.de](mailto:f.kreppel@uni-mainz.de)

Christian Melzer: [chmelzer@uni-mainz.de](mailto:chmelzer@uni-mainz.de)

Janis Wagner: [wjanis@students.uni-mainz.de](mailto:wjanis@students.uni-mainz.de)

Janine Hilder: [hilder@uni-mainz.de](mailto:hilder@uni-mainz.de)

Ulrich Poschinger: [poschin@uni-mainz.de](mailto:poschin@uni-mainz.de)

Ferdinand Schmidt-Kaler: [fsk@uni-mainz.de](mailto:fsk@uni-mainz.de)

André Brinkmann: [brinkman@uni-mainz.de](mailto:brinkman@uni-mainz.de)

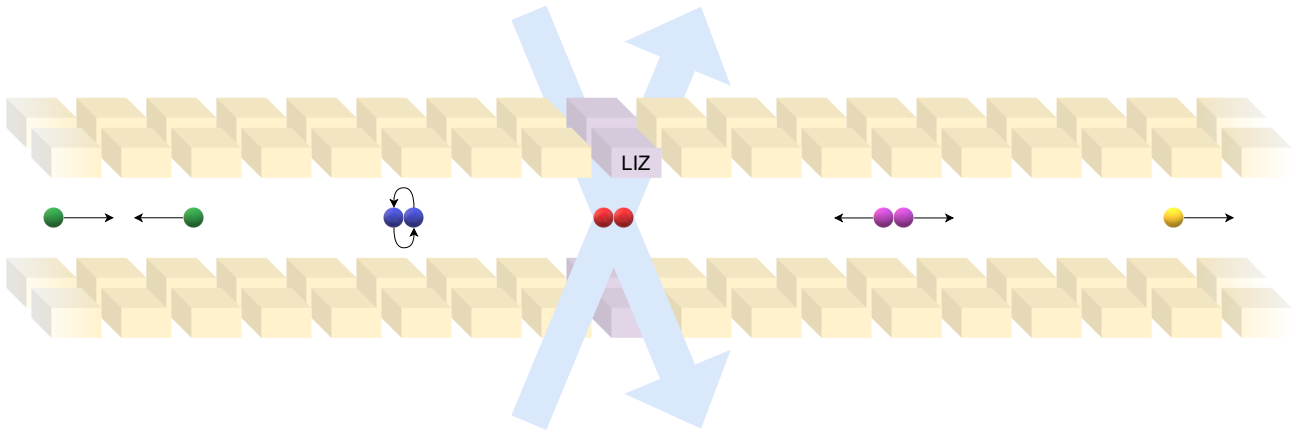


Fig. 1: Linear shuttling-based segmented ion trap architecture: The ions are stored in small groups at different segments of the architecture. The lasers performing the gate operations (here, on the red ions) are only directed to one specific segment, the laser interaction zone (LIZ, purple segment). The following operations can reconfigure the ion positions (from left to right): Merging ions into a new group (green ions), physically swapping ions (blue ions), splitting a group (purple ions) and translating ions between different segments (yellow ion).

ating schedules of shuttling operations based on the compilation result is handled by a subsequent *Shuttling Compiler* stage [9, 10, 11, 12], which is beyond the scope of this work.

This manuscript is structured as follows: [Sec. 2](#) reviews existing circuit optimization techniques. [Sec. 3](#) defines the representation of quantum circuits used in this work. This is followed by a detailed description of all utilized circuit transformation algorithms in [Sec. 4](#). An evaluation of the methods is presented in [Sec. 5](#) and shows the benefits of the circuit compiler.

## 2 Background

Due to the increasing size and complexity of quantum circuits, circuit compilation is an active research field. Since the circuit compilation is essential to make algorithms portable and execute quantum circuits on different platforms, powerful frameworks for quantum computing [13, 14, 15] were developed. While the features of these are notably different, all frameworks offer built-in optimization.

While the simplest form of circuit compilation replaces gates by predefined sequences of other gates (often referred to as a decomposition), more advanced techniques serve to minimize the number of gates. A common strategy is the reduction of overall gate count with special focus on expensive two-qubit gates [16, 17, 18]. There are various ways to achieve such a gate count reduction. One possibility is the utilization of a different circuit representation called ZX-calculus [19], which allows for simplifications on the functional level. A different approach uses templates, where common circuit patterns are searched and replaced by a shorter or otherwise preferable, but functionally identical gate sequences [18].

When compiling quantum circuits, also the qubit

mapping is often considered. Ideally, each qubit can interact with every other qubit, such that two-qubit gates can be executed between each pair of qubits. However, for existing platforms, interactions are restricted to nearest-neighbor topology or full connectivity within subsets of limited size. Mapping the qubits from the algorithmic circuit to physical qubits subjected to these hardware restrictions is called the routing problem [13]. To render arbitrary two-qubit gates executable on the quantum hardware, SWAP gates have to be inserted into the circuit using heuristics [20, 21, 22, 23]. In case of ion trap quantum computers, ion positions can be physically swapped to establish dynamical all-to-all connectivity. Consequently, no computational SWAP gates have to be inserted at this stage.

The Cambridge Quantum Computing’s Pytket framework [13] offers a wide variety of circuit transformation algorithms and is therefore used as the operational basis for the custom circuit compiler described in this work. Functionality like the removal of redundancies as well as the rebasing of arbitrary gates into the native gate set is realized mainly using built-in functions of Pytket. Since Pytket is designed for superconducting architectures, some specific functionalities for trapped-ion quantum computers were additionally developed and implemented. This includes the concatenation of multiple local rotations into global rotations, restricting gate parameters to a fixed set of values and improving the gate order.

## 3 Graph description of the quantum circuit

In this section a quantum circuit is described as directed acyclic graph (DAG), which is the data structure Pytket and our custom subroutines work on. The

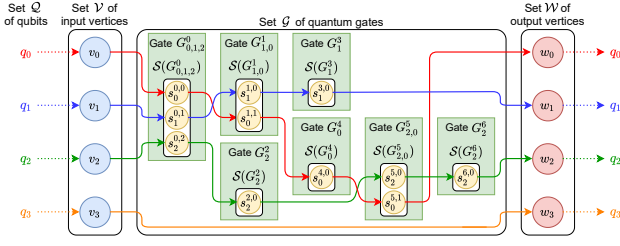


Fig. 2: Example of a quantum circuit's graph with four qubits and seven gates. The four qubits are depicted on both sides and every qubit  $q_i$  is assigned to its input node  $v_i$ . In the middle are the gates which are executed on the qubits. Each gate has as many subnodes as qubits the gate is acting on. On the right side are the output nodes for each qubit. The directed edges show in which order the gates are executed on each qubit represented by the different edge colors. No gate is executed on qubit  $q_3$ .

first subsection defines the DAG and in the second subsection the DAG is constructed. Such a graph is depicted in Fig. 2. At the end of this section, we describe the native gate set of our platform.

### 3.1 Graph definition

We consider a quantum circuit consisting of a set  $\mathcal{Q} = \{q_0, \dots, q_{n-1}\}$  of  $n$  qubits. The circuit is represented as directed acyclic graph  $C = (\mathcal{V} \cup \mathcal{G} \cup \mathcal{W}, \mathcal{E})$  with sets of vertices  $\mathcal{V}$ ,  $\mathcal{G}$  and  $\mathcal{W}$  which are pairwise disjoint and defined as follows:

- $\mathcal{V}$  is the set of input vertices. For every qubit  $q_i \in \mathcal{Q}$  exists exactly one vertex  $v_i \in \mathcal{V}$ , so  $|\mathcal{V}| = n$  applies. Every vertex  $v_i$  has exactly one outgoing edge.
- $\mathcal{G}$  is the set of the circuit's quantum gates. If a quantum gate operates on  $m \geq 1$  different qubits  $q_{i_0}, \dots, q_{i_{m-1}} \in \mathcal{Q}$ , the vertex will have exactly  $m$  incoming and  $m$  outgoing edges. Additionally, every gate  $G \in \mathcal{G}$  depends on  $a \geq 0$  parameters, which are angle parameters with values of  $0 \leq \phi_0, \dots, \phi_{a-1} < 2\pi$ . In the following, a gate  $G$  acting on the qubits  $q_{i_0}, \dots, q_{i_{m-1}}$  and depending on the parameters  $\phi_0, \dots, \phi_{a-1}$  is denoted as

$$G_{i_0, \dots, i_{m-1}}^j(\phi_0, \dots, \phi_{a-1}) \quad (1)$$

where  $j$  is a unique identifier for the gate.

- $\mathcal{W}$  is the set of output vertices. For every qubit  $q_i \in \mathcal{Q}$  exists exactly one vertex  $w_i \in \mathcal{W}$ , so  $|\mathcal{W}| = n$  applies. Every vertex  $w_i$  has exactly one incoming edge.

### 3.2 Graph construction

Each quantum circuit  $C$  starts with the input vertices  $v_0, \dots, v_{n-1} \in \mathcal{V}$ . Every qubit  $q_i \in \mathcal{Q}$  is assigned to its vertex  $v_i$ . The outgoing edge  $(v_i, G) \in \mathcal{E}$  leads to the

vertex  $G \in \mathcal{G}$  that represents the quantum gate which is executed first on  $q_i$ . If the circuit does not contain any quantum gate executed on  $q_i$ , the outgoing edge will lead directly to the output vertex  $w_i \in \mathcal{W}$  so that  $(v_i, w_i) \in \mathcal{E}$  applies.

All nodes in  $\mathcal{G}$  represent the inner nodes of the circuit  $C$ . If a gate  $G^j \in \mathcal{G}$  is executed directly before a gate  $G^k \in \mathcal{G}$  on the same qubit  $q_i$ ,  $G^j$  and  $G^k$  will be connected by one directed edge  $(G^j, G^k) \in \mathcal{E}$ .

The end of the circuit  $C$  is built by the output vertices  $w_0, \dots, w_{n-1} \in \mathcal{W}$ . Every qubit  $q_i \in \mathcal{Q}$  is assigned to its vertex  $w_i$ . The incoming edge  $(G, w_i) \in \mathcal{E}$  comes from the vertex  $G \in \mathcal{G}$  that represents the quantum gate which is executed last on  $q_i$ . If the circuit does not contain any quantum gate executed on  $q_i$ , the incoming edge will come directly from the input vertex  $v_i \in \mathcal{V}$ .

In contrast to the input and output vertices, which have all exactly one outgoing or one incoming edge, the inner nodes have  $m \geq 1$  incoming and outgoing edges. To manage these edges, every inner vertex  $G^j \in \mathcal{G}$  consists of  $m$  subnodes  $s^{j,0}, \dots, s^{j,m-1}$ . Each of these subnodes has exactly one incoming and one outgoing edge. The set of the subnodes of  $G^j$  is denoted as  $\mathcal{S}(G^j)$  in the following.

Assume  $G^j, G^k, G^l$  with  $G^j \in \mathcal{V} \cup \mathcal{G}$ ,  $G^k \in \mathcal{G}$  and  $G^l \in \mathcal{G} \cup \mathcal{W}$  are executed sequentially on a qubit  $q_i \in \mathcal{Q}$ , so that the edges  $e_{\text{in}} = (G^j, G^k), e_{\text{out}} = (G^k, G^l) \in \mathcal{E}$  exist. Instead of directly connecting the incoming edge  $e_{\text{in}}$  to  $G^k$ , it is connected to a subnode  $s^{k,\alpha} \in \mathcal{S}(G^k)$ . The outgoing edge  $e_{\text{out}}$  starts on the same subnode  $s^{k,\alpha}$ . Each subnode has only one incoming and outgoing edge. If  $G^k$  is a controlled gate, the  $m-1$  control qubits are connected to the subnodes  $s^{k,0}, \dots, s^{k,m-2}$  and the target qubit to the subnode  $s^{k,m-1}$ . Because only  $q_i$  is connected to the subnode  $s^{k,\alpha}$ , the subnode can be denoted as  $s_i^{k,\alpha}$ .

After constructing the complete graph, there are  $n$  disjoint, clearly defined paths in  $C$  beginning on one input vertex  $v_i \in \mathcal{V}$  and ending at a output vertex  $w_i \in \mathcal{W}$ . Every path from  $v_i$  to  $w_i$  describes the order in which the gates are applied to qubit  $q_i \in \mathcal{Q}$ . An example of a graph representation of a quantum circuit is shown in Fig. 2.

### 3.3 Native gate set

The state of an  $n$  qubit register is commonly represented by a normalized complex-valued vector with  $2^n$  entries, corresponding to the probability amplitudes of the logical basis states. The gates then act as unitary transformations on the state, which are represented by unitary matrices of dimension  $2^n \times 2^n$ .

The serial execution of gates on different qubits is represented by products of unitary operators or the corresponding matrices, where the products are read from right to left. Note that we employ a less strict notation throughout the manuscript, where operator

products are written as simple products albeit the operators might act on different subsets of the qubit register and tensor products are not always written explicitly. Since global phases of the quantum states do not affect measurement outcomes, equality of unitaries and states denotes equality up to a global phase. To execute the circuit  $C$  on a given hardware platform, it must be transformed to an equivalent circuit consisting only of gates from a native gate set. Our platform [8] implements the native gate set

$$\mathcal{M} = \{\mathbf{R}(\theta, \phi), \mathbf{Rz}(\phi), \mathbf{ZZ}(\theta)\}. \quad (2)$$

where each gate is parameterized using up to two rotation angles  $\theta$  and  $\phi$  with  $0 \leq \theta, \phi < 2\pi$ . In the following they will be also referred to as the pulse area and the phase, respectively, due to their meaning for the actual operation. The gates from  $\mathcal{M}$  are defined as follows in terms of the Pauli operators  $X$ ,  $Y$  and  $Z$ :

$$\mathbf{R}(\theta, \phi) = \exp\left(-i\frac{\theta}{2}(\cos\phi X + \sin\phi Y)\right) \quad (3a)$$

$$\mathbf{Rz}(\phi) = \exp\left(-i\frac{\phi}{2}Z\right) \quad (3b)$$

$$\mathbf{ZZ}(\theta) = \exp\left(-i\frac{\theta}{2}Z \otimes Z\right). \quad (3c)$$

The gates  $\mathbf{R}$  and  $\mathbf{Rz}$  are single qubit gates, whereas  $\mathbf{ZZ}$  is a two-qubit gate. This set is complete, such that any quantum algorithm can be decomposed into a sequence of these operations [24, 25]. Note that some trapped-ion platforms do not allow for native  $\mathbf{ZZ}$  gates, but rather employ  $\mathbf{XX}$  gates generated by bichromatic radiation fields [26]. Our compilation scheme is still valid for such architectures, as  $\mathbf{ZZ}$  gates can be generated from  $\mathbf{XX}$  gate using local wrapper rotations. Furthermore, the identity  $\mathbf{I}$ , the Pauli gates  $\mathbf{X}$ ,  $\mathbf{Y}$ ,  $\mathbf{Z}$  and rotations around  $X$  and  $Y$ ,  $\mathbf{Rx}$  and  $\mathbf{Ry}$ , are special forms of the  $\mathbf{R}$  and  $\mathbf{Rz}$  gates and therefore also part of the native gate set. Their relation to the gates in  $\mathcal{M}$  is

$$\mathbf{I} = \mathbf{R}(0, \phi) \quad (4a)$$

$$\mathbf{Rx}(\theta) = \mathbf{R}(\theta, 0) \quad (4b)$$

$$\mathbf{Ry}(\theta) = \mathbf{R}\left(\theta, \frac{\pi}{2}\right) \quad (4c)$$

$$\mathbf{X} = i\mathbf{Rx}(\pi) \quad (4d)$$

$$\mathbf{Y} = i\mathbf{Ry}(\pi) \quad (4e)$$

$$\mathbf{Z} = -\mathbf{Rz}(\pi) \quad (4f)$$

A peculiar feature of the shuttling-based platform concerns  $\mathbf{SWAP}$  gates, defined as

$$\mathbf{SWAP} = \frac{1}{2}(\mathbf{I} \otimes \mathbf{I} + \mathbf{X} \otimes \mathbf{X} + \mathbf{Y} \otimes \mathbf{Y} + \mathbf{Z} \otimes \mathbf{Z}) \quad (5)$$

While these gates, required to establish full effective connectivity, could be realized using the logical gates contained in  $\mathcal{M}$ , they are removed from circuits upon compilation and reintroduced in a following compilation stage, which is discussed in Sec. 4.1. Instead of

laser-driven  $\mathbf{SWAP}$  gates, physical ion swapping is used to reconfigure the qubit registers. This process is advantageous as it does not require manipulate of the internal qubits states and therefore can be executed at unit fidelity [27, 28, 29].

On our platform, all gate operations from (3) are realized via laser pulses, and the rotation angle parameters  $\theta$  correspond to pulse areas, i. e. integrals of intensity over time. In order to perform gate operations at high fidelities, these pulse areas must be carefully calibrated. We therefore restrict the set of available gates to rotation angles equal to the pre-calibrated pulse areas  $\theta = \pi$  and  $\theta = \frac{\pi}{2}$  for  $\mathbf{R}$  gates and  $\frac{\pi}{2}$  for  $\mathbf{ZZ}$  gates. Note that there is no restriction on the rotation angle  $\theta$  for the  $\mathbf{Rz}$  gates. Concatenated application of  $\mathbf{R}$  gates allows for all pulse area multiples of  $\frac{\pi}{2}$ . The phases  $\phi$  of the gates can be chosen arbitrarily at a resolution only limited by hardware capabilities. These considerations lead to a restriction of the gate set to:

$$\mathcal{N} = \left\{\mathbf{R}\left(\frac{\pi}{2}, \phi\right), \mathbf{R}(\pi, \phi), \mathbf{Rz}(\phi), \mathbf{ZZ}\left(\frac{\pi}{2}\right)\right\}. \quad (6)$$

In the following sections, the individual transformations leading to a circuit entirely comprised of elements of  $\mathcal{N}$  will be described.

## 4 Transformations

The overall goal of a quantum compiler is to modify and rearrange gates in a given quantum circuit in order to obtain an equivalent circuit with reduced total gate count and more favorable operations in terms of the execution resources fidelity and runtime. The following section describes the transformations applied to the input circuit  $C$  for converting into a circuit comprised only of gates from the allowed gate set  $\mathcal{N}$ , composed in a way minimizing the execution overhead on a shuttling-based platform. For some of the following transformations, the built-in functions of the quantum programming framework Pytket [13] are used. An overview over all compilation steps and the corresponding set of gates is shown in Fig. 3. In the same order, each compilation step will be described in a subsection. In general, transformations impacting the circuit structure on a large scale are applied earlier while local adjustments are applied at later stages to preserve optimized structures of previous steps. Throughout this section, we assume the input circuit  $C$  to consist only of quantum gates defined within Pytket [30]. This means that all high-level sub-circuits, e. g., a Quantum Fourier transform, are substituted by Pytket-defined quantum gates before applying the following transformations. A circuit which contains gates not being part of the restricted native gate set  $\mathcal{N}$  and deals as an example throughout this section is depicted in Fig. 4.

In addition to Pytket's built-in algorithms, the characteristics of the segmented ion trap architecture are

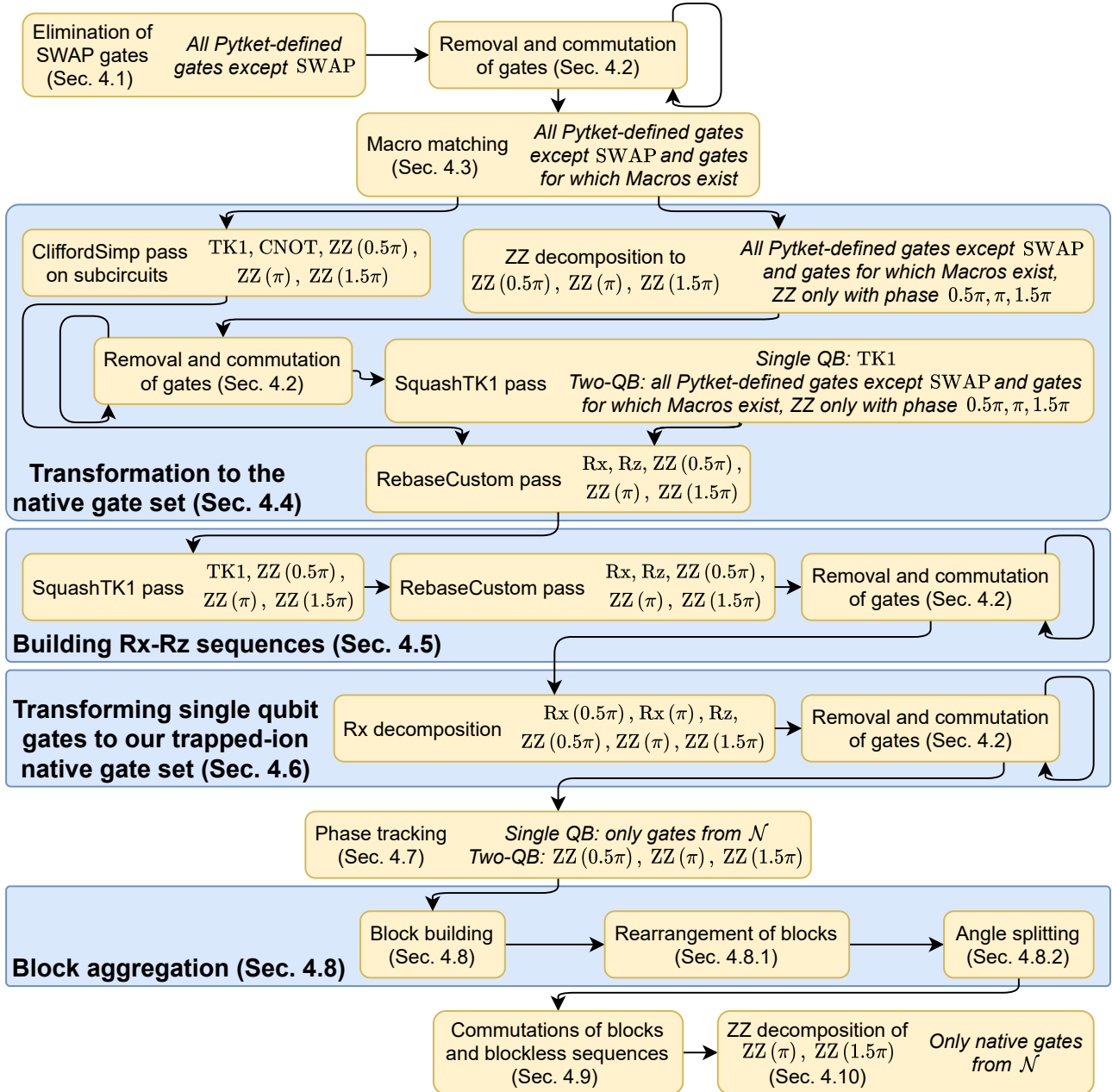


Fig. 3: Compilation flow of our compiler. Each yellow box represents one transformation step of the compilation process. In the boxes are noted either only the name of the transformation step or the name of the transformation step on the left hand side and the gate set of which the circuit consists after the transformation on the right hand side. The blue boxes bundle several transformation steps to larger logical steps, each of which are described in one section.

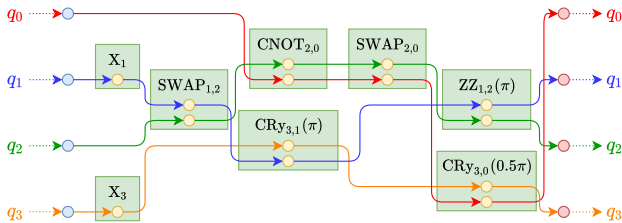


Fig. 4: Example of a graph representation of a quantum circuit with four qubits. The circuit contains gates not being part of the restricted native gate set  $\mathcal{N}$ .

taken into account. Most importantly, gates are always executed simultaneously on all ion qubits stored at the laser interaction zone. This enables parallel execution of two local qubit rotations R.

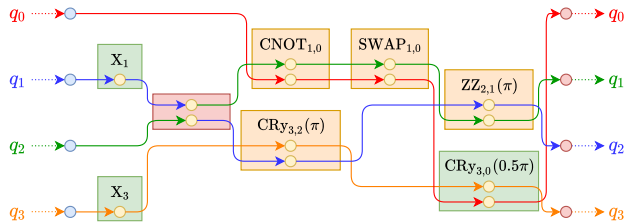
#### 4.1 Elimination of SWAP gates

Our shuttling-based ion trap quantum computer natively supports physically swapping ions [27, 28, 29], required for establishing effective full connectivity between the ion qubits. In contrast to other gates, SWAP gates are carried out by physically swapping ions. Thus, the function of SWAP gates is replaced by renaming the qubits for all succeeding operations. It is the task of the Shuttling Compiler further downstream in the software stack to generate the corresponding reconfiguration operations.

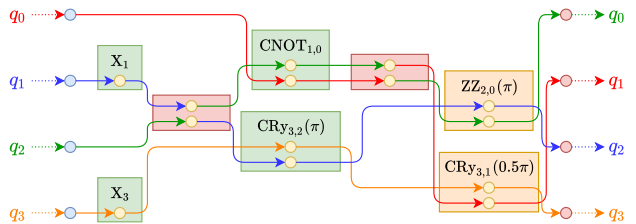
The process of SWAP gate elimination on the circuit from Fig. 4 is shown in Fig. 5. In order to eliminate the SWAP gates the elimination algorithm iterates over the gates  $G \in \mathcal{C}$  in their executing order. When  $G$  is a  $\text{SWAP}_{i,j}^k$  gate acting on the qubits  $q_i$  and  $q_j$ ,  $G$  has two subnodes  $s_i^{k,0}$  and  $s_j^{k,1}$ , respectively. The algorithm exchanges the outgoing edges of these two subnodes. This means that on  $q_i$  all gates are applied which are on the path from the input node  $v_i$  to  $\text{SWAP}_{i,j}^k$ . Because the outgoing edges of  $s_i^{k,0}$  and  $s_j^{k,1}$  were exchanged, after  $\text{SWAP}_{i,j}^k$   $q_i$  follows the path original followed by  $q_j$ . The same holds for  $q_j$  which follows after  $\text{SWAP}_{i,j}^k$  the path original followed by  $q_i$ . Consequently, all gates after  $\text{SWAP}_{i,j}^k$  which were original executed on  $q_j$  are now executed on  $q_i$  and vice versa. In this way the swap is passed through all gates succeeding  $\text{SWAP}_{i,j}^k$ , and  $\text{SWAP}_{i,j}^k$  can be eliminated from the circuit.

#### 4.2 Repeated removal and commutation of gates

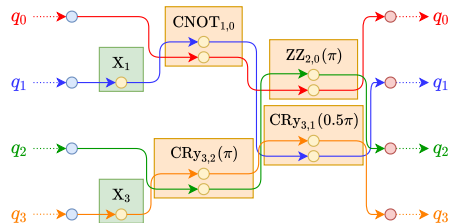
To reduce the total gate count, after some transformations it is tested whether the circuit contains redundant gates or gate sequences. For this purpose, Pytket's `RemoveRedundancies` pass is used. Additionally, Pytket's `CommuteThroughMultis` pass is executed to commute gates. When applying commutations, single qubit gates are commuted through



(a) The SWAP gate elimination is applied on the first SWAP gate (the red box). Compared to Fig. 4 the outgoing edges are exchanged. This means that after the SWAP gate,  $q_1$  is following the green path and  $q_2$  the blue one. Consequently, the qubits on which the CNOT $_{2,0}$ , CRY $_{3,1}(\pi)$ , SWAP $_{2,0}$  and ZZ $_{1,2}(\pi)$  gates from Fig. 4 are acting on must be adapted to the new qubit following the path. Because all gates which are on the path of  $q_1$  and  $q_2$  after the SWAP gate are adapted to the new qubit following the path, the SWAP gate can be eliminated from the circuit.



(b) The SWAP gate elimination is also applied on the second SWAP gate (the right red box). Consequently, the outgoing edges are exchanged compared to panel (a). This means that after the SWAP gate,  $q_0$  follows the green path and  $q_1$  the red one. Because the CRY $_{3,0}(\frac{\pi}{2})$  gate from panel (a) is adapted to  $q_1$  following the red path and the ZZ $_{2,1}(\pi)$  gate to  $q_0$  following the green path, the SWAP gate can be eliminated from the circuit.



(c) The circuit after applying the SWAP gate elimination: With the elimination of the SWAP gates, the orange gates now operate on different qubits than in Fig. 4.

Fig. 5: Example from Fig. 4 when applying the SWAP gate elimination.

two-qubit gates wherever possible. This may again give rise to redundant gates, which can then be removed. Procedures of commutation and removing are repeated until the total gate count does not further decrease.

This transformation step is first executed after eliminating the SWAP gates and will be applied after some of the later transformation stages as well. It conserves the property of a gate sequence being in gate set  $\mathcal{M}$  or being in gate set  $\mathcal{N}$  up until multiples of  $\frac{\pi}{2}$ .

#### 4.3 Macro Matching

Although Pytket contains a transformation for arbitrary gates into the native gate set  $\mathcal{M}$ , which will be utilized in Sec. 4.4, a custom decomposition might

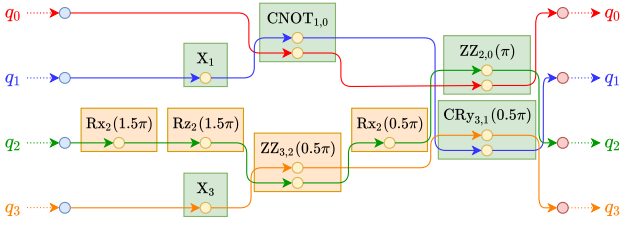


Fig. 6: Example from Fig. 5c with the macro matching applied. Because only the gate  $\text{CRy}_{3,2}(\pi)$  of the  $\text{CRy}$  gates in Fig. 5c satisfies the condition  $\theta = \ell\pi$  with  $\ell \in \mathbb{Z}$ , only this gate is substituted by the orange gates.

yield better results. Therefore, in this step, for several gates or gate sequences, a predefined decomposition into the native gate set – termed *macro matching* – is applied to the quantum circuit. This is especially useful for large structured circuits, where known structures can be replaced by beneficial alternatives. The macro matching transformation is carried out only for gates acting on  $m \geq 2$  qubits, as efficient transformations of local rotations  $m = 1$  exist, (see Sec. 4.4). Let  $\mathcal{L}$  be a set of gates for which an efficient decomposition is known. All gates from  $C$  contained in  $\mathcal{L}$  are substituted by a sequence of gates from  $\mathcal{M}$ . The gate sequence of the macro is defined in a way that it can be described by the same unitary matrix as the gate  $G$ , up to a global phase. An example for such a macro is

$$\begin{aligned} \text{CRy}_{i,j}(\theta) &= \exp\left(-\frac{i}{4}\theta(1 - Z_1)Y_2\right) \\ &= \text{Rx}_j\left(\frac{\pi}{2}\right) \text{ZZ}_{i,j}\left(\frac{\theta}{2}\right) \text{Rz}_j\left(-\frac{\theta}{2}\right) \text{Rx}_j\left(-\frac{\pi}{2}\right). \end{aligned} \quad (7)$$

Due to the angle restrictions of the gates in  $\mathcal{N}$ , this macro is only applied if  $\theta = \ell\pi$  with  $\ell \in \mathbb{Z}$  holds. Otherwise, the original  $\text{CRy}$  gate remains in the circuit and will be substituted via the transformations in Sec. 4.4. To simplify the circuit the repeated removal and commutation of gates from Sec. 4.2 is executed again. It is depicted in Fig. 6 how the macro matching is applied to the circuit from Fig. 5c.

#### 4.4 Transformation to the native gate set

The predefined gate decomposition into the native gate set via macro matching is followed by the conversion of all remaining gates into the native gate set. For this transformation, two different approaches can be employed. In the first approach, Pytket’s `CliffordSimp` pass is applied to the quantum circuit  $C$ , which contains simplifications similar to Duncan and Fagan [31]. After applying the `CliffordSimp` pass on a circuit, the resulting circuit consists only of Pytket’s universal single qubit TK1 gates and two-qubit CNOT gates, which are defined as follows:

$$\text{TK1}_i(\alpha, \beta, \gamma) = \text{Rz}_i(\alpha) \text{Rx}_i(\beta) \text{Rz}_i(\gamma) \quad (8a)$$

$$\text{CNOT}_{ij} = \exp\left(i\frac{\pi}{4}(I - Z_i)(I - X_j)\right). \quad (8b)$$

Because the `CliffordSimp` pass also converts ZZ gates with  $\theta \in \{\frac{\pi}{2}, \pi, \frac{3\pi}{2}\}$  already contained in  $C$  to a sequence of several TK1 and CNOT gates, it is not directly applied to the entire circuit  $C$ , but is executed on sub-circuits of  $C$  such that ZZ gates with  $\theta \in \{\frac{\pi}{2}, \pi, \frac{3\pi}{2}\}$  are preserved. This is advantageous because ZZ  $(\frac{\pi}{2})$  gates are already part of the restricted native gate set  $\mathcal{N}$  and thus this gate sequence would not become shorter. Similarly, ZZ  $(\pi)$  as well as ZZ  $(\frac{3\pi}{2})$  gates can also be transformed with a smaller gate count, see Sec. 4.10. The result when applying the `CliffordSimp` pass on the example from Fig. 6 can be seen in Fig. 7a.

As it will be seen in Sec. 5, the `CliffordSimp` pass has a non-linear runtime in the number of gates. To make even large circuits transformable in a reasonable time, we developed an alternative approach to convert an arbitrary gate sequence to the given native gate set uses Pytket’s `SquashTK1` pass which simplifies single qubit gate sequences. Because this pass does not change the two-qubit gates and the built-in rebasing routine employed in the following paragraph does not allow to restrict the rotation angles to the ones contained in the restricted native gate set, all ZZ gates in  $C$  with  $\theta \notin \{\frac{\pi}{2}, \pi, \frac{3\pi}{2}\}$  must be substituted manually. For that purpose the following decomposition is used:

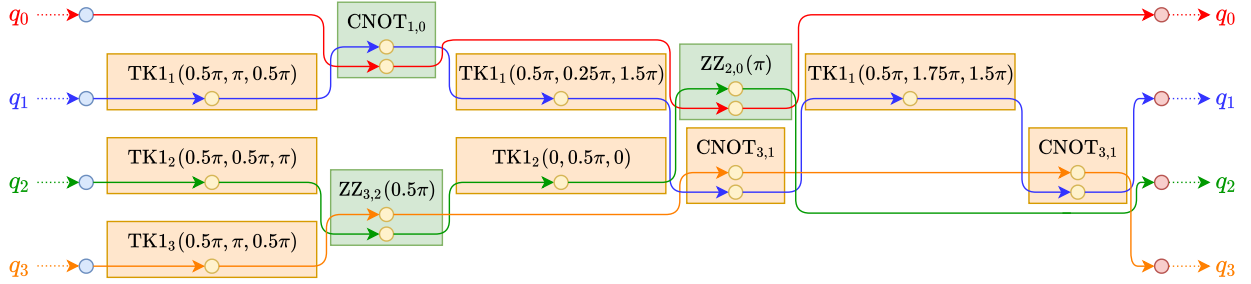
$$\begin{aligned} \text{ZZ}_{i,j}(\theta) &= \text{Rz}_j\left(\frac{\pi}{2}\right) \text{Rx}_j\left(\frac{\pi}{2}\right) \text{ZZ}_{i,j}\left(\frac{\pi}{2}\right) \\ &\quad \cdot \text{Rz}_j(\pi) \text{Rx}_j(-\theta) \text{ZZ}_{i,j}\left(\frac{\pi}{2}\right) \\ &\quad \cdot \text{Rx}_j\left(\frac{3\pi}{2}\right) \text{Rz}_j\left(\frac{3\pi}{2}\right) \text{Rz}_i(\pi). \end{aligned} \quad (9)$$

After the substitution, the repeated removal and commutation of gates from Sec. 4.2 is executed again to simplify the circuit. Following, Pytket’s `SquashTK1` pass is applied, which converts every sequence of single qubit gates to exactly one TK1 gate. Applying these substitutions on the example from Fig. 6 results in the circuit shown in Fig. 7b.

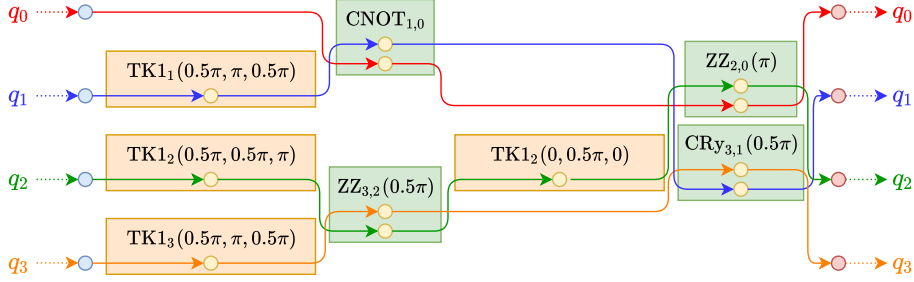
For either approach used, the gates in  $C$  are subsequently transformed to the gates in the set  $\{\text{Rx}, \text{Rz}, \text{ZZ}\}$ . This process is called *rebasing*. The transformation is executed using Pytket’s `RebaseCustom` pass. We found smaller gate counts when excluding the Ry gate, thus we excluded Ry from the set. Because the circuit  $C$  can contain two-qubit gates which are not ZZ gates when using the second approach described above, the rebasing first substitutes all two-qubit gates not being ZZ gates to sequences of TK1 and CNOT gates and subsequently rebases the TK1 gates by the definition from (8a) and the CNOT gates to

$$\begin{aligned} \text{CNOT}_{i,j} &= \text{Rz}_j\left(\frac{\pi}{2}\right) \text{Rx}_j\left(\frac{\pi}{2}\right) \text{Rz}_j\left(\frac{\pi}{2}\right) \text{Rz}_i\left(\frac{\pi}{2}\right) \\ &\quad \cdot \text{ZZ}_{i,j}\left(\frac{\pi}{2}\right) \text{Rx}_j\left(\frac{\pi}{2}\right) \text{Rz}_j\left(\frac{\pi}{2}\right) \\ &\quad \cdot \text{Rx}_i\left(\frac{\pi}{2}\right) \text{Rz}_i(\pi) \text{Rx}_i\left(\frac{\pi}{2}\right). \end{aligned} \quad (10)$$

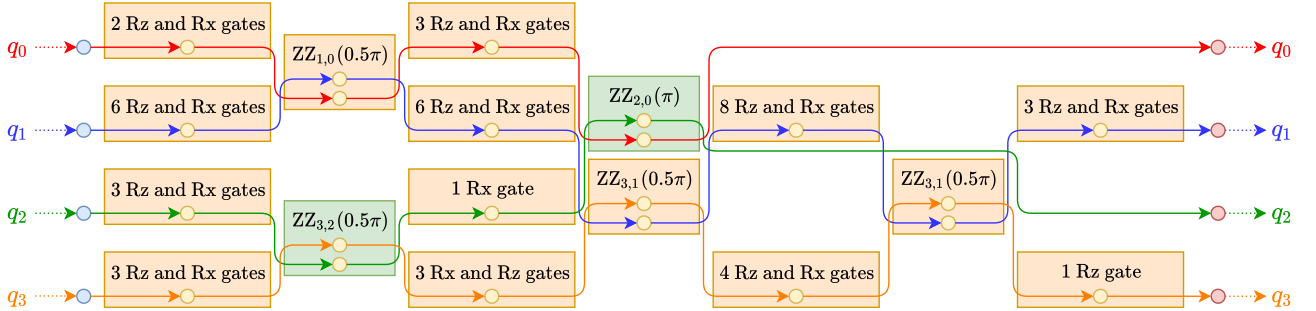
The decomposition guarantees that only ZZ gates with an angle of  $\theta = \frac{\pi}{2}$  are introduced into  $\mathcal{G}$  so that after applying this transformation, all ZZ gates have an



(a) Example from Fig. 6 after applying Pytket's CliffordSimp pass as described in Sec. 4.4. All sequences of single qubit gates were substituted by exactly one TK1 gate. Moreover, the  $\text{CRY}_{3,1}(\pi)$  gate in Fig. 6 was transformed to the two orange  $\text{CNOT}_{3,1}$  gates and additional TK1 gates. Because the CliffordSimp pass is executed so that ZZ gates with  $\theta \in \{\frac{\pi}{2}, \pi, \frac{3\pi}{2}\}$  are not converted,  $\text{ZZ}_{3,2}(\frac{\pi}{2})$  and  $\text{ZZ}_{2,0}(\pi)$  remains in the circuit.



(b) Example from Fig. 6 after applying Pytket's SquashTK1 pass as described in Sec. 4.4. Here also all sequences of single qubit gates were substituted by exactly one orange TK1 gate. In contrast to the CliffordSimp pass the green two-qubit gates stayed unchanged.



(c) Circuit after applying Pytket's RebaseCustom pass as described in Sec. 4.4 on the circuits from the panels (a) and (b). In this case both circuits result in the same transformed circuit containing only gates from the gate set  $\mathcal{M}$ . Each CNOT gate was transformed to exactly one orange ZZ gate and 11 Rz and Rx gates. Additionally, each TK1 gate was substituted by exactly three Rz and Rx gates. Because the ZZ gate is an element of the gate set  $\mathcal{M}$ , the green ZZ gate is the only gate remaining unchanged.

Fig. 7: The process of transforming a circuit to the gate set  $\mathcal{M}$ .

angle  $\theta \in \{\frac{\pi}{2}, \pi, \frac{3\pi}{2}\}$ . After applying the `RebaseCustom` pass on the circuits from [Fig. 7a](#) and [Fig. 7b](#) the circuit in [Fig. 7c](#) results.

#### 4.5 Building Rx-Rz sequences

At this point, the quantum circuit contains only `R` and `Rz` gates with arbitrary angle parameters as single qubit gates and `ZZ` gates with an angle parameter of  $\frac{\ell\pi}{2}$  as two-qubit gates. This makes the gate set of the quantum circuit gates compatible with the native gate set  $\mathcal{M}$ . Since any arbitrary sequence of single qubit gates can be compactly represented by exactly one `TK1` gate, the first step is to reduce every sequence of concatenated single qubit gates into a `TK1` gate. Such sequences start and end at either two-qubit gates or at input or output vertices  $v_i, w_i$ . The implementation of the algorithm is Pytket's `SquashTK1` pass. It is depicted in [Fig. 8a](#) how this algorithm is applied to the circuit from [Fig. 7c](#). Then, Pytket's `RebaseCustom` pass is used to transform the `TK1` gates into gates of set  $\mathcal{M}$  using [\(8a\)](#). It is instructive to write down the circuit unitary reduced to all gates acting along the path of qubit  $q_i$ , which assume the following form:

$$U_i = \left( \prod_{\lambda=0}^{\omega_i-1} \text{Rz}_i \text{Rx}_i \text{Rz}_i \text{ZZ}_{i,j(\lambda)} \right) \text{Rz}_i \text{Rx}_i \text{Rz}_i. \quad (11)$$

In this expression,  $\omega_i$  is the number of `ZZ` gates executed on  $q_i$  and  $j(\lambda)$  stands for the qubit  $q_{j(\lambda)}$  on which the `ZZ` gate  $\lambda$  also acts. The circuit from [Fig. 8a](#) in which each path has the above form after applying the transformation is shown in [Fig. 8b](#).

Each `ZZ` gate  $\text{ZZ}_{i,j}^k \in C$  is now sandwiched by two `Rz` gates, which commute with the  $\text{ZZ}_{i,j}^k$  gate, on both qubits  $q_i$  and  $q_j$ . Therefore, we can commute the succeeding `Rz` gates through the `ZZ` gates and merge with the preceding `Rz` gates:

$$\text{Rz}_i(\phi_s) \text{ZZ}_{i,j(\lambda)} \text{Rz}_i(\phi_p) \rightarrow \text{ZZ}_{i,j(\lambda)} \text{Rz}_i(\phi_s + \phi_p). \quad (12)$$

Repeating this procedure combined with the elimination of redundant gates until no further reduction of the number of gates is possible as described in [Sec. 4.2](#) results in a circuit  $C$  in which the disjoint paths of each qubit  $q_i \in \mathcal{Q}$  have the following form:

$$U_i = \left( \prod_{\lambda=0}^{\omega_i-1} \text{Rz}_i \text{Rx}_i \text{ZZ}_{i,j(\lambda)} \right) \text{Rz}_i \text{Rx}_i \text{Rz}_i. \quad (13)$$

Consequently, on each qubit  $q_i$  at most one `Rx` and one `Rz` gate are executed between two `ZZ` gates. Let

$$\omega = \frac{1}{2} \sum_{i=0}^{n-1} \omega_i \quad (14)$$

be the number of `ZZ` gates in  $\mathcal{G}$ . Hence,  $\mathcal{G}$  consists exactly of  $\omega$  two-qubit gates and at most  $4\omega + 3n$

single qubit gates. It is shown in [Fig. 8c](#) how this transformation is applied to the circuit from [Fig. 8b](#). `Rx` and `Rz` with arbitrary angles are the only remaining single qubit gates in the circuit and both are also part of  $\mathcal{M}$ . Since also all remaining two-qubit gates are part of that set, all gates  $G_i$  of the circuit now fulfill  $G_i \in \mathcal{M}$ .

#### 4.6 Transforming single qubit gates to our trapped-ion native gate set

Since all gates in the circuit are now part of  $\mathcal{M}$ , the next step is to make the angles compliant with the restricted native gate set  $\mathcal{N}$ , which has restrictions to the allowed rotation angles. Therefore, all `Rx` gates must have  $\theta \in \{\frac{\pi}{2}, \pi\}$ . Two trivial conversions can be executed for  $\theta = 0$  and  $\theta = \frac{3\pi}{2}$ . In the first case the gate is equal to the `I` gate and can thus be eliminated. In the second case the gate can be substituted by  $\text{Rx}(\frac{\pi}{2}) \text{Rx}(\pi)$ .

Rotations `Rx` with any other values of  $\theta$  are required to be converted into a sequence of `Rx` gates with allowed rotation angles and `Rz` gates with freely variable rotation angles. We employ the decomposition

$$\begin{aligned} & \text{Rx}(\theta) \\ &= \text{Rz}\left(\frac{\pi}{2}\right) \text{Rx}\left(\frac{\pi}{2}\right) \text{Rz}(\theta + \pi) \text{Rx}\left(\frac{\pi}{2}\right) \text{Rz}\left(\frac{\pi}{2}\right). \end{aligned} \quad (15)$$

After this substitution, the restrictions of the restricted native gate set  $\mathcal{N}$  are fulfilled for the single qubit gates. It is shown in [Fig. 9a](#) how the circuit from [Fig. 8c](#) is transformed.

Because this transformation is directly applied after the creation of `Rx-Rz` sequences in [Sec. 4.5](#), the unitaries pertaining to the disjoint paths of each qubit  $q_i$  assume the following form:

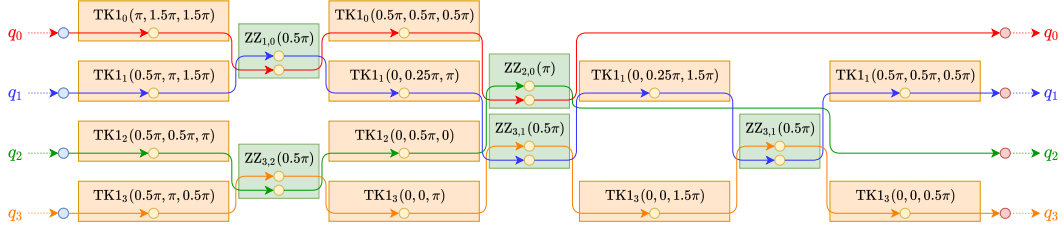
$$\begin{aligned} U_i = & \left( \prod_{\lambda=0}^{\omega_i-1} \text{Rz}_i \text{Rz}_i \text{Rx}_i \text{Rz}_i \text{Rx}_i \text{Rz}_i \text{ZZ}_{i,j(\lambda)} \right) \\ & \cdot \text{Rz}_i \text{Rz}_i \text{Rx}_i \text{Rz}_i \text{Rx}_i \text{Rz}_i \text{Rz}_i. \end{aligned} \quad (16)$$

By again commuting `Rz` gates through `ZZ` and combining consecutive `Rz` gates according to [\(12\)](#) using the procedures from [Sec. 4.2](#), the expression can be simplified to

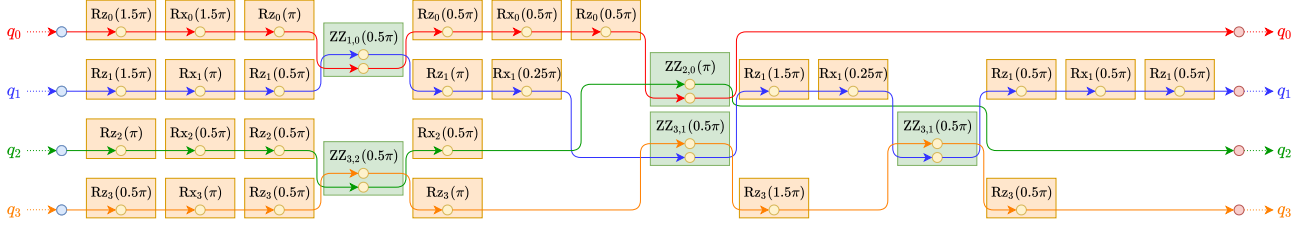
$$\begin{aligned} U_i = & \left( \prod_{\lambda=0}^{\omega_i-1} \text{Rz}_i \text{Rx}_i \text{Rz}_i \text{Rx}_i \text{ZZ}_{i,j(\lambda)} \right) \\ & \cdot \text{Rz}_i \text{Rx}_i \text{Rz}_i \text{Rx}_i \text{Rz}_i. \end{aligned} \quad (17)$$

Consequently, on each qubit  $q_i$  at most two `Rx` and two `Rz` gates are executed between two `ZZ` gates. Let  $\omega$  be the number of `ZZ` gates in  $\mathcal{G}$  as defined in [\(14\)](#). Hence,  $\mathcal{G}$  consists exactly of  $\omega$  two-qubit gates and at most  $8\omega + 5n$  single qubit gates. It is depicted in [Fig. 9b](#) how this transformation is applied to the circuit from [Fig. 9a](#).

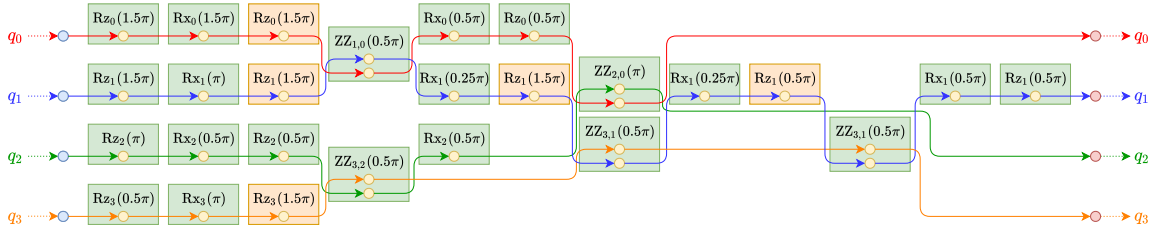
Since all `R(x)` gates now fulfill  $\theta \in \{\frac{\pi}{2}, \pi\}$ , all single qubit gates are now part of the restricted native gate set  $\mathcal{N}$ .



(a) Example from Fig. 7c after applying Pytket's SquashTK1 pass. Each single qubit gate sequence was transformed to exactly one orange TK1 gate.

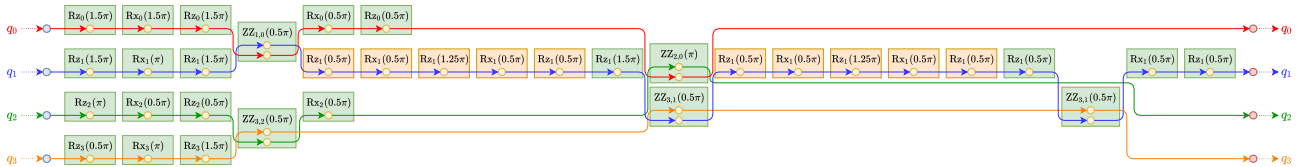


(b) Circuit after applying Pytket's RebaseCustom pass on the circuit from the panel (a). Each TK1 gate was transformed to the TK1 decomposition consisting of three gates. Because the angles of some gates from the decomposition are 0 and thus these gates are equal to the identity gate, some decomposition have less than three gates.

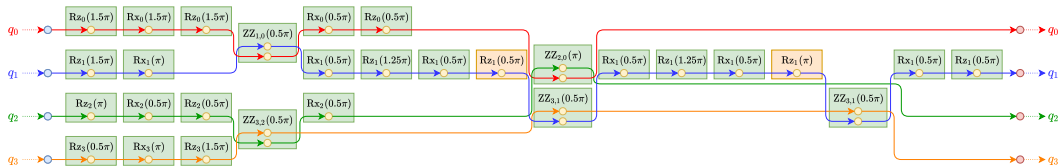


(c) Circuit from panel (b) after the Rz gates were commuted through the ZZ gates and the resulting redundancies were removed. Consequently, there are at most two single qubit gates between two ZZ gates on each qubit  $q_i$  and between the last gate executed on  $q_i$  and the output node of  $q_i$ . Only between the input node of  $q_i$  and the first gate executed on  $q_i$  three single qubit gates are possible.

Fig. 8: The process of building Rx-Rz sequences.



(a) Example from Fig. 8c after applying the transformation of single qubit gates to the restricted native gate set. The two  $RX_1(0.25\pi)$  gates in Fig. 8c are transformed to the two orange gate sequences and their angles are contained in the phase of the  $RZ_1(1.25\pi)$  gates. All single qubit gates of the circuit are in the restricted native gate set  $\mathcal{N}$ .



(b) Circuit from panel (a) after the Rz gates were commuted through the ZZ gates and the resulting redundancies were removed. Because the transformation is applied directly after the building of the Rx-Rz sequences there are at most four single qubit gates between two ZZ gates on each qubit  $q_i$  and between the last gate executed on  $q_i$  and the output node of  $q_i$ . Only between the input node of  $q_i$  and the first gate executed on  $q_i$  five single qubit gates are possible.

Fig. 9: The process of transforming the single qubit gates to the restricted native gate set  $\mathcal{N}$ .

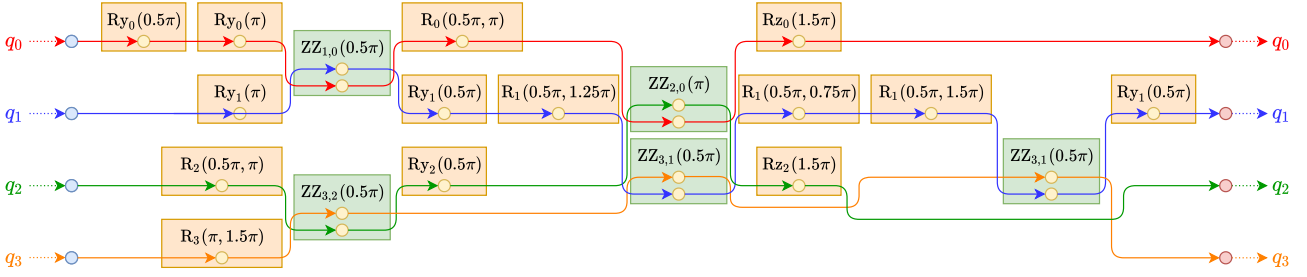


Fig. 10: Example of Fig. 9b after applying the phase tracking algorithm on the circuit. For each Rx gate, the graph contains an R gate depending on the angle of the original gate and the value of the tracking phase  $b_i$  when executing the algorithm on qubit  $q_i$ . The R gates can be simplified to Rx or Ry gates if  $b_i = 0$  or  $b_i = \frac{\pi}{2}$ , respectively. The graph does not contain Rz gates any more except between the last R gate executed on each qubit  $q_i$  and the output node of  $q_i$ . Consequently, there are at most two R gates between two ZZ gates on each qubit  $q_i$  and between the input node of  $q_i$  and the first gate executed on  $q_i$ . Only between the last gate executed on  $q_i$  and the output node of  $q_i$  two R gates and one Rz gate are possible. Because the value of tracking phase  $b_0$  is 0 after applying the algorithm on qubit  $q_1$  and  $q_3$ , there is no Rz gate placed before the output nodes of  $q_1$  and  $q_3$ .

## 4.7 Phase tracking

We now utilize that a gate Rz followed by a gate R is equivalent to a single R gate with a phase shifted by the rotation angle of the Rz gate:

$$R(\theta, \phi)Rz(\theta_z) = R(\theta, \phi - \theta_z). \quad (18)$$

Combined with the fact that Rz gates commute through ZZ gates this allows for *virtual* execution of all Rz gates using the well-known approach called *phase tracking* [32, 7]. This technique avoids any physical execution of Rz gates and is therefore beneficial in terms of overall runtime and fidelity. All R gates contained in  $C$  have to be modified in terms of their phase arguments according to the procedure outlined in the following.

The algorithm initializes a tracking phase  $b_i = 0$  for every qubit  $q_i \in \mathcal{Q}$  and follows its path from input vertex  $v_i \in \mathcal{V}$  to output vertex  $w_i \in \mathcal{W}$ . The following rules are applied to each gate  $g \in C$  encountered:

- If  $G_i = R_i(\theta, \phi)$ ,  $G_i$  is substituted by  $R_i(\theta, \phi - b_i)$
- If  $G_i = Rz_i(\phi)$ ,  $G_i$  is removed from  $C$  and the value of  $b_i$  is changed to  $b_i + \phi$

An additional gate  $Rz_i(b_i)$  is inserted into  $C$  directly before  $w_i$ , correcting for the final accumulated phase. Since the Rz gate does only change the phase of the qubit, the measurement result in the computational basis as performed on the hardware would not be affected. However, adding the Rz gate still has advantages when working with the unitary matrix and when using the circuit as a building block for even larger circuits. An example can be seen in Fig. 10.

Because the phase tracking algorithm is directly executed after the transformation of Sec. 4.6, the disjoint paths of each qubit  $q_i \in \mathcal{Q}$  assume the following form:

$$U_i = Rz_i \left( \prod_{\lambda=0}^{\omega_i-1} R_i R_i ZZ_{i,j}(\lambda) \right) R_i R_i. \quad (19)$$

Note that the subsequent R gates can generally not be merged as they have different phase parameters. Thus, on each qubit at most two R gates are executed between ZZ gates. Hence,  $\mathcal{G}$  consists exactly of  $\omega$  two-qubit gates and at most  $4\omega + 3n$  single qubit gates. Consequently, phase tracking can almost halve the number of single qubit gates.

Since only phases, but not pulse areas, are changed, still all single qubit gates are part of  $\mathcal{N}$ .

## 4.8 Block aggregation

In this section, we describe further optimization steps which are specific to our shuttling-base architecture. Here, the ions are stored in a linear segmented trap, where qubit subsets are stored at different trap segments. The qubit sets can be rearranged between gate operation via shuttling operations [8, 6]. All gate operations are carried out by laser beams directed to a fixed location, the laser interaction zone. Here, any gate operation is carried out simultaneously on all ions stored. Identical single qubit gates can be executed in parallel on multiple qubits. Now we will use this to reduce the number of gates. As an additional constraint, we keep the shuttling operations at a minimum. Thus single qubit operations are only parallelized on qubits already situated in the same segment, i.e. before or after performing a two-qubit gate on them.

The optimization described in this section deals with the aggregation of single qubit gates. It uses the property that there is a specific structure around certain ZZ gates. Directly before and/or directly after a ZZ gate  $ZZ_{i,j}^k$ , there can be sequences of preceding single qubit gates  $p = (p_0, \dots, p_{\alpha-1}), p_0, \dots, p_{\alpha-1} \in C$  and/or succeeding single qubit gates  $s = (s_0, \dots, s_{\beta-1}), s_0, \dots, s_{\beta-1} \in C$  which are similar on both qubits  $q_i, q_j \in \mathcal{Q}$  on which the gate  $ZZ_{i,j}^k$  is acting on. This means that in these sequences the gates as well as the angle parameters

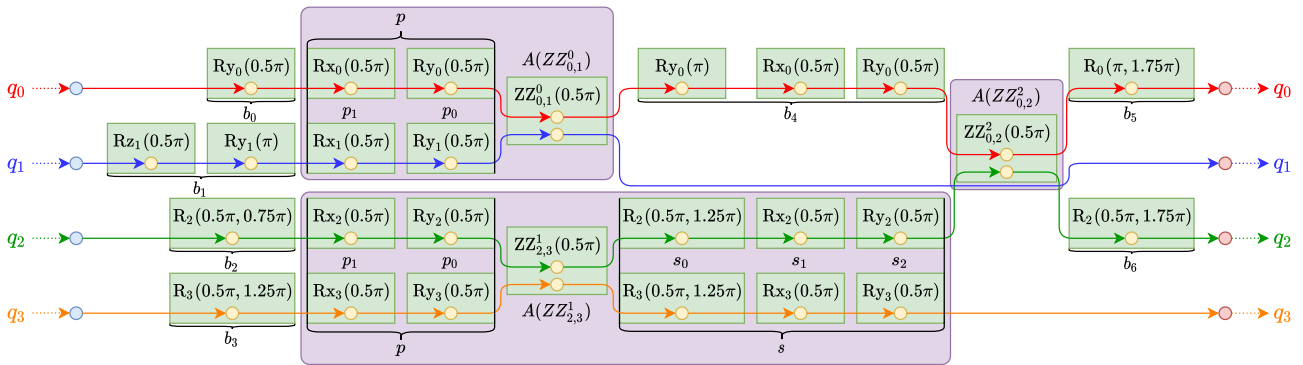


Fig. 11: An example circuit with the blocks built by the algorithm from Sec. 4.8. Because the graph contains three ZZ gates, it also contains three blocks represented by the purple boxes around the ZZ gates. Each block  $A(ZZ_{i,j}^k)$  can have a predecessor sequence  $p$  and/or successor sequence  $s$ . The block  $A(ZZ_{0,2}^2)$  contains neither a sequence  $p$  nor a sequence  $s$  and consists only of the ZZ gate. Beside the three blocks, the graph consists of the seven blockless sequences  $b_0$  to  $b_6$ .

exactly match on  $q_i$  and  $q_j$ . The advantage of these sequences is that the gates  $p_0, \dots, p_{\alpha-1}, s_0, \dots, s_{\beta-1}$  can be executed simultaneously for both qubits  $q_i$  and  $q_j$  rather than being executed sequentially for each qubit, which reduces the execution time and the required shuttling overhead. Every ZZ gate including the single qubit gates contained in the sequences  $p$  and  $s$  make up one block  $A$ . The block pertaining to  $ZZ_{i,j}^k$  is denoted as  $A(ZZ_{i,j}^k)$  in the following.

Iterating over all ZZ gates in their execution order, for every gate  $ZZ_{i,j}^k$  the algorithm will look if  $q_i$  and  $q_j$  undergo an identical single qubit gate  $G_p$  directly before  $ZZ_{i,j}^k$ . If this is the case and  $G_p$  does not already belong to another block on  $q_i$  or  $q_j$ ,  $G_p$  will be added to the predecessor sequence  $p$  of block  $A(ZZ_{i,j}^k)$  and the procedure is repeated with the gate directly before  $G_p$ . Otherwise  $p$  cannot be increased. The same procedure is repeated with the gates directly after  $ZZ_{i,j}^k$  to build the sequence  $s$  of  $A(ZZ_{i,j}^k)$ . Because the ZZ gates are traversed in their execution order, it is guaranteed that candidate gates for  $s$  do not already belong to another block. If it is not possible to build  $p$  and  $s$ , the block will consist only of  $ZZ_{i,j}^k$ .

An example of the block building process is depicted in Fig. 11. After building such blocks around every ZZ gate  $ZZ^k \in C$ , there can exist gate sequences  $b_0, \dots, b_{\ell-1}$  which do not belong to one block. Each of these blockless sequences consists only of single qubit gates and pertains to exactly one qubit. The aim is now to minimize the number  $\ell$  of the blockless sequences.

To minimize the amount and length of blockless single qubit sequences, the blocks can be rearranged and single qubit gates can be split. These two approaches will be discussed in the following two subsections.

#### 4.8.1 Rearrangement of blocks

Block rearrangement is possible if before a sequence  $p$  of a block  $A_\alpha$ , both qubits  $q_i$  and  $q_j$  undergo the same gate  $G$ , but for one qubit, e. g.,  $q_j$ ,  $G$  already belongs

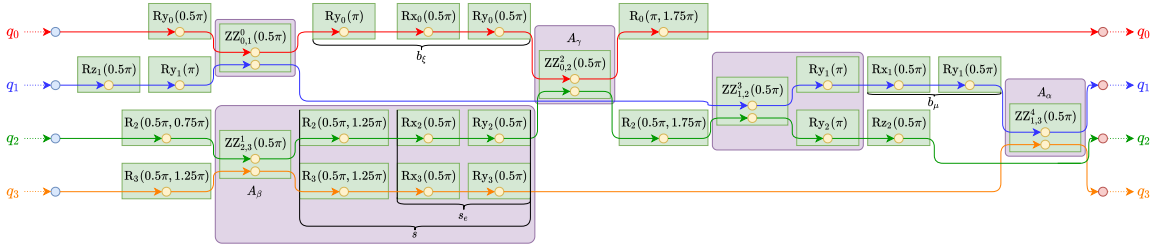
to a preceding block  $A_\beta$  and for  $q_i$ , it belongs to a blockless sequence  $b_\mu$ . Assume  $A_\beta$  operates on the qubit  $q_j$  and a third qubit  $q_k$ . If the entire blockless sequence  $b_\mu$  is equal to the end  $s_e$  of the sequence  $s$  of block  $A_\beta$ , the gates of  $b_\mu$  and  $s_e$  acting on qubit  $q_j$  will be appended at the front of the sequence  $p$  of  $A_\alpha$ . Consequently, the blockless sequence  $b_\mu$  is eliminated and the gates of  $q_j$  in  $s_e$  are removed from  $s_e$ , see Fig. 12a and Fig. 12b.

Because only the gates of qubit  $q_j$  in  $s_e$  are removed from  $s_e$ , the gates of qubit  $q_k$  in  $s_e$  now give rise to a new blockless sequence  $b_\nu$ . To eliminate  $b_\nu$ , it is necessary that  $b_\nu$  borders on a third block  $A_\gamma$  operating on qubit  $q_k$  and a qubit  $q_l$ . Here, the case  $q_i = q_l$  is possible. If before the sequence  $p$  of  $A_\gamma$  there exists a blockless sequence  $b_\xi$  on qubit  $q_l$  containing the sequence  $b_\nu$  on its end  $b_{\xi_e}$ ,  $b_\nu$  and  $b_{\xi_e}$  will be appended at the front of  $p$  of  $A_\gamma$  and the number of blockless segments on the circuit will be minimized by one. This can be seen in Fig. 12b and Fig. 12c. If a minimization of the number of blockless sequences is not possible, because a matching sequence is missing during the algorithm, the blocks will not be rearranged. The rearranging procedure is repeated for all blocks on which rearrangement is possible.

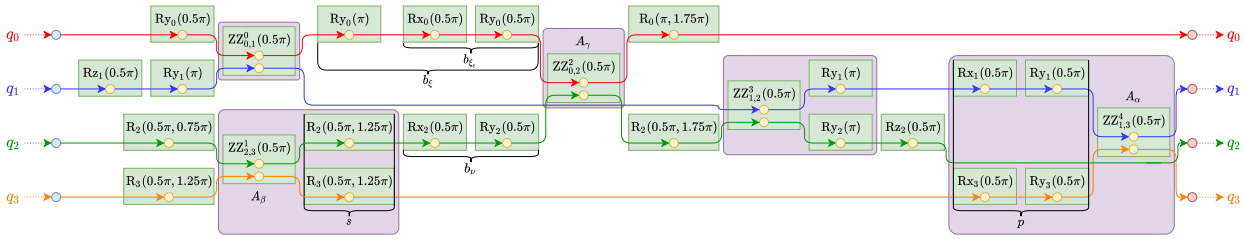
#### 4.8.2 Angle splitting

After the rearrangement, the number of blockless sequences might be further reduced by splitting the rotation angles of certain gates. Assume that before a sequence  $p$  or directly after a sequence  $s$  of a block  $A(ZZ_{i,j}^k)$ , both qubits  $q_i$  and  $q_j$  undergo rotations  $R_i(\theta_i, \phi)$  and  $R_j(\theta_j, \phi)$  with the same phase angle but different rotation angles. Then, it is possible to split the gate with the larger rotation angle into two rotations, merge the resulting two identical gates into the respective set  $s$  or  $p$  of the block and eventually reduce the number of blockless sequences. The phase angle will be omitted from the notation in the following.

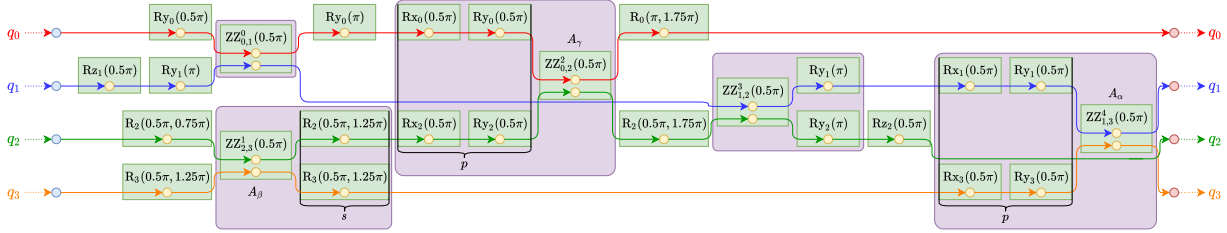
We now assume  $G_i(\theta_i)$  to belong to the blockless se-



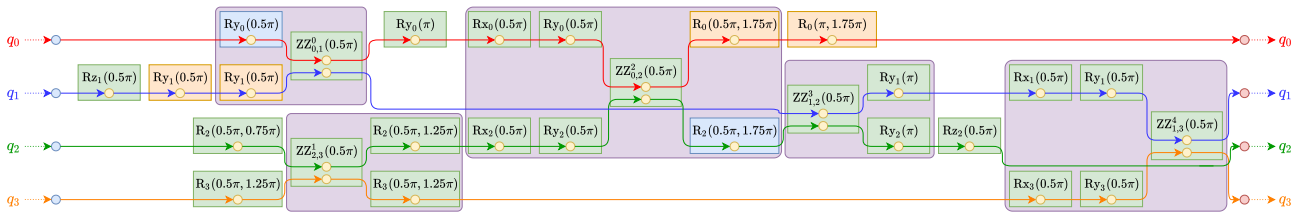
(a) Before the block  $A_\alpha$  the same gate sequences  $b_\mu$  and  $s_e$  are executed on the qubits  $q_1$  and  $q_3$ . On  $q_1$  the gate sequence  $b_\mu$  is a blockless sequence while on  $q_3$  the gate sequence  $s_e$  belongs to another block  $A_\beta$ . To eliminate the blockless sequence  $b_\mu$ ,  $b_\mu$  and the gates on  $q_3$  from  $s_e$  can be added as predecessor sequence to  $A_\alpha$ .



(b)  $b_\mu$  and the gates on  $q_3$  from  $s_e$  were added as predecessor sequence  $p$  to  $A_\alpha$ . Consequently, the gates on  $q_2$  from  $s_e$  build now a new blockless sequence  $b_\nu$ . This blockless sequence is identical to the blockless sequence  $b_\xi$  on qubit  $q_1$ . Because  $b_\nu$  and  $b_\xi$  are both directly before a third block  $A_\gamma$ , they can be added as predecessor sequence to  $A_\gamma$ .



(c)  $b_\mu$  and  $b_\xi$  were added as predecessor sequence  $p$  to  $A_\gamma$ . Through the rearranging of the blocks the graph has now one blockless sequence less than in panel (a).



(d) In panel (c) before the block of the gate  $ZZ_{0,1}^0$  and after the block of the gate  $ZZ_{0,2}^2$  the same gates are executed, but with different pulse areas  $\theta$ . When applying the angle splitting approach, the gate with the greater angle is substituted by the two orange gates. Because the gate next to the block as well as the blue gate have the same angle, these two gates can be added to the block. In this way two blockless sequences are eliminated. On the two R gates before the block of gate  $ZZ_{1,3}^1$  the angle splitting approach cannot be applied because the phase  $\phi$  differs.

Fig. 12: The process of rearranging blocks and splitting angles.

quence  $b_i$  and  $G_j(\theta_j)$  to the blockless sequence  $b_j$ , and both  $b_i$  and  $b_j$  are directly either preceding or succeeding block  $A$ . We further assume without loss of generality that  $\theta_i < \theta_j$ . The gate  $G_j(\theta_j)$  can be split into two subsequent gates  $G_j(\theta_i)$   $G_j(\theta_j - \theta_i)$ , such that a simultaneous gate  $G(\theta_i)$  can be merged to either  $p$  or  $s$ . In the former case,  $G(\theta_i)$  will be appended at the front of  $p$ , while in the latter case,  $G(\theta_i)$  will be appended at the end of  $s$ . In both cases,  $G_i(\theta_i)$  is eliminated from  $b_i$  and within  $b_j$ ,  $G_j(\theta_j)$  is substituted by  $G_j(\theta_j - \theta_i)$ . In this way the blockless sequence  $b_i$  is reduced by one gate and can be eliminated if the sequence is now empty. If this is not the case and  $b_i$  cannot be eliminated, the transformation step is rejected and the initial gates  $G_i(\theta_i)$  and  $G_j(\theta_j)$  are retained. The procedure is repeated until no block  $A$  can be increased any more. The execution of the angle splitting approach on the circuit from Fig. 12c is shown in Fig. 12d.

Afterwards, all sequences  $b$  which cannot be eliminated completely are transformed according to Sec. 4.4, such that they consist of a minimal number of native gates from  $\mathcal{N}$ . The same transformations are applied to the sequences  $p$  and  $s$  of each block  $A$  to minimize the number of used gates.

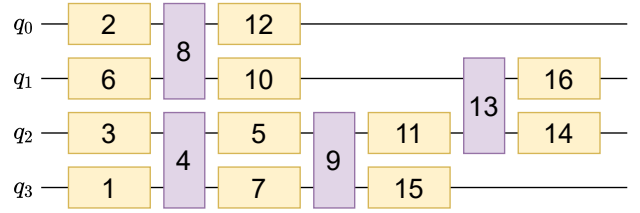
Note that before the angle splitting step, the circuit consists only of gates with rotation angles  $\theta \in \{\frac{\pi}{2}, \pi\}$ , therefore the angle splitting preserves the property that all gates are contained in the set of allowed gates  $\mathcal{N}$ .

#### 4.9 Commutations of blocks and blockless sequences

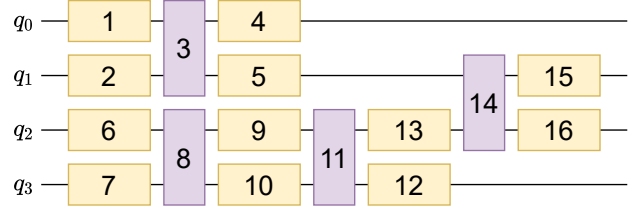
Now, commutations of blocks and blockless sequences are used to reduce the number of required shuttling operations. Blocks and blockless sequences are rearranged, which facilitates the work for the subsequent Shuttling Compiler stage. There are two different commutations, which will be described in the following. An example of the commutation rules is depicted in Fig. 13.

The first commutation deals with the order of blocks: If two blocks  $A_\alpha$  and  $A_\beta$  are executed on the qubits  $q_i, q_j$  and in between no other block is executed neither on any of those qubits, then  $A_\alpha$  and  $A_\beta$  are commuted such that between them only blockless sequences acting on  $q_i$  or  $q_j$  are executed. The order in which these two blockless sequences are executed is not relevant since it does not influence the total count of required shuttling operations. This commutation affects the Blocks 8 and 11 in Fig. 13b. Both blocks are applied on the qubits  $q_2$  and  $q_3$ . Between these two blocks no other block and only the blockless sequences 9 and 10 are executed.

The second commutation sorts the order of the remaining blockless sequences: Blockless sequences acting on  $q_i$  and  $q_j$  are commuted so that they are both



(a) The gates are enumerated in a semi-random order only paying attention that on each qubit  $q_i$  a gate  $G$  is executed after all gates placed before  $G$  on  $q_i$  have been executed.



(b) The commutations of Sec. 4.9 have been applied. Blockless sequences of a qubit  $q_i$  are always executed directly before or after a block acting on  $q_i$ . Between the Blocks 8 and 11 acting on  $q_2$  and  $q_3$  no other block and only blockless sequences acting on  $q_2$  and  $q_3$  are executed. Because Block 14 is the next block after Block 11 and both gates act on qubit  $q_2$ , the blockless sequences applied after Block 11 are ordered so that the sequence on qubit  $q_3$  is executed before the sequence on qubit  $q_2$ . Consequently, the sequence on qubit  $q_2$  is executed directly before the Block 14.

Fig. 13: Example of applying commutations on a circuit. The purple boxes represent blocks and the yellow boxes blockless sequences. The numbers inside the boxes specify in which order the gates are executed, i. e. the gate with the number 1 is executed first, then the gate with number 2 and so on.

executed directly before or after a block  $A_\alpha$  which acts on these two qubits. If the next block  $A_\beta$  executed after  $A_\alpha$  also acts on  $q_i$ , but not on  $q_j$ , then the blockless sequence of  $q_j$  will be moved directly after  $A_\alpha$  and before the blockless sequence of  $q_i$ . The same rule holds if  $A_\beta$  acts on  $q_j$ , but not on  $q_i$ , correspondingly. If  $A_\beta$  acts neither on  $q_i$  nor  $q_j$  then the order of the single qubit gate may be arbitrary. The case in which  $A_\beta$  acts on  $q_i$  and  $q_j$  is discussed in the previous paragraph. This commutation affects Block 3 in Fig. 13b, which is executed on the qubits  $q_0$  and  $q_1$ . Directly before Block 3 the blockless sequences 1 and 2 and directly after Block 3 the blockless sequences 4 and 5 are executed. All these blockless sequences act on  $q_0$  or  $q_1$ , respectively. The execution order of the sequences 1 and 2 is not strictly defined. The next block which is executed after Block 3 on  $q_0$  or  $q_1$  is Block 14. Because Block 14 is only applied to  $q_1$  out of these two qubits, the blockless sequence 4 on  $q_0$  is executed before the blockless sequence 5 on  $q_1$ .

#### 4.10 Transformation of two-qubit gates to our trapped-ion native gate set

During the transformation in Sec. 4.4, the ZZ gates are converted so that they have a phase  $\theta \in \{\frac{\pi}{2}, \pi, \frac{3\pi}{2}\}$ . Because the native gate set  $\mathcal{N}$  only contains the gate

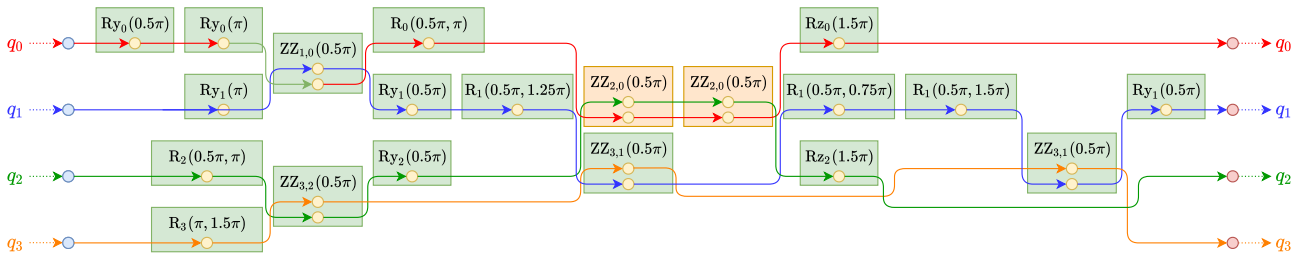


Fig. 14: Example from Fig. 10 after applying the transformation of two-qubit gates to the restricted native gate set. The  $\text{ZZ}_{2,0}(\pi)$  gate in Fig. 10 is transformed to the two orange  $\text{ZZ}_{2,0}(\frac{\pi}{2})$  gates. All gates of the circuit are in the restricted native gate set  $\mathcal{N}$ .

$\text{ZZ}(\frac{\pi}{2})$ , the ZZ gates with a phase of  $\pi$  or  $\frac{3\pi}{2}$  or must be transformed so that the condition is satisfied. Therefore the following decomposition is used:

$$\text{ZZ}(\pi) = \text{ZZ}(\frac{\pi}{2}) \text{ZZ}(\frac{\pi}{2}) \quad (20a)$$

$$\text{ZZ}(\frac{3\pi}{2}) = \text{ZZ}(\frac{\pi}{2}) \text{ZZ}(\frac{\pi}{2}) \text{ZZ}(\frac{\pi}{2}). \quad (20b)$$

This transformation is applied to the circuit from Fig. 10 in Fig. 14.

Note, that this transformation could also have been applied earlier. However, not only would that not have any benefits but it would also worsen the block aggregation runtime as there are more two-qubit gates to consider. It shall also be mentioned that the single qubit gates are already part of the restricted native gate set and since the two-qubit gates are so, too, the circuit is now executable on the target quantum computing architecture.

## 5 Evaluation

In this section, the evaluation results of our compiler are presented. We test the compiler for a library of 149 quantum circuits [33] which were previously used for benchmarks [20, 21, 22, 23]. Each circuit has between 3 and 16 qubits and 5 to 125,362 gates. The evaluations were executed on a notebook with an Intel Core i7-10750H CPU and 16 GB RAM. We evaluated the impact of the different compilation stages on the result. Additionally, our compiler is compared to standard Pytket [13] and Qiskit [15] passes as well as the results of the Pytket’s *pytket-aqt* extension [34]. This extension was developed by the company AQT targeting an ion trap quantum computer [35]. We employ Pytket version 1.1.0, Qiskit version 0.36.1 and *pytket-aqt* version 0.19.0. We always determine the runtime averaged over 10 executions of a given circuit. The resulting single qubit and two-qubit gate counts are shown in App. A.

All circuits were executed using the compilation flow depicted in Fig. 3. For the macro matching of Sec. 4.3, only the  $\text{CRy}$  macro given in (7) was used. Since we presented two alternative ways of transforming to the native gate set, as discussed in Sec. 4.4, these approaches are compared. While the

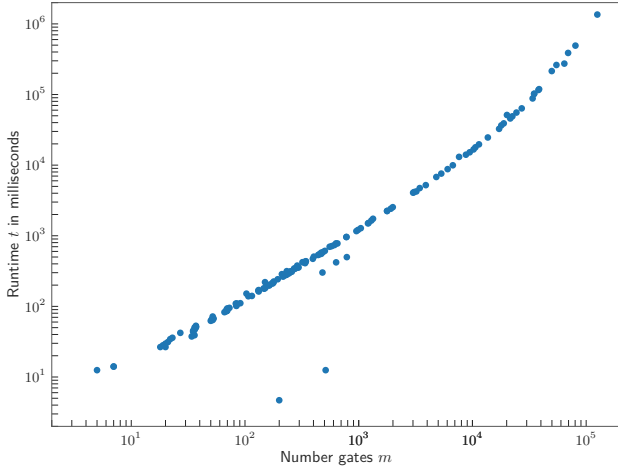
first scheme performs additional optimizations using Pytket’s *CliffordSimp* pass, the second scheme transforms based on the ZZ decomposition from (9) and Pytket’s *SquashTK1* pass without further optimizations. The two different approaches are visualized in Fig. 3, where they constitute the left and the right control paths, respectively, in the uppermost blue box. In the following, these two schemes will be referred to as the *CliffordSimp* and *SquashTK1* approaches.

In the following, first the impact of the different transformation will be analyzed. Afterwards, our compiler will be compared to Pytket, AQT and Qiskit.

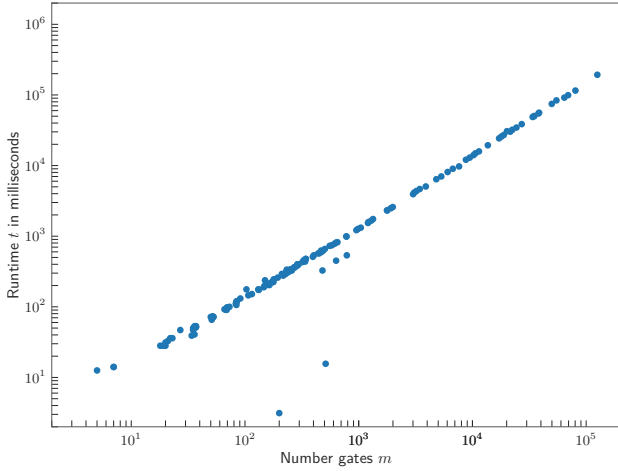
### 5.1 Analysis of the impact of the different transformations

When analyzing the results, the *CliffordSimp* approach usually produces between 0.96 and 1.40 times lower gate counts for the circuits than the *SquashTK1* approach. The single qubit gate count of the *CliffordSimp* approach is between 0.94 and 1.35 times less, while the two-qubit gate count is between 1.00 and 1.50 times less, which means that the two-qubit gate count of the *CliffordSimp* approach is never higher than the one of the *SquashTK1* approach. 97% of the compiled circuits exhibit a higher overall gate count as compared to the original circuits, as all transformed circuits ought to comply with the restricted native gate set  $\mathcal{N}$ . However, the number of two-qubit gates in the transformed circuits never exceeds the count corresponding to the original circuit. The reason for this is that the original circuits contain some redundant CNOT gates, which can be removed after commuting the single qubit gates between them, and each remaining CNOT gate is substituted by exactly one ZZ gate using the decomposition from (10). Two of the five circuits with lower gate count after transformation are *qft\_10* and *qft\_16* which were transformed to empty circuits by the *CliffordSimp* approach as well as *SquashTK1* approach.

The runtime of the *CliffordSimp* and *SquashTK1* approaches versus the number of gates in the original circuit is shown in Fig. 15. The *SquashTK1* approach lead to mostly constant compile time of about 1.35 ms



(a) In this benchmark our CliffordSimp approach was used. It can be clearly seen that the optimization leads to a non-linear runtime scaling.



(b) In this benchmark our SquashTK1 approach was used. In contrast to our CliffordSimp approach in panel (a), this routine behaves linearly in the number of gates.

Fig. 15: Runtime of our compiler depending on the number of gates. Every point represents one circuit of the benchmark.

per gate of the original circuit. In contrast to this, the CliffordSimp approach displays a non-linear growth of the compile time with the number of gates in the original circuit. The reason for this are the additional optimizations executed by Pytket’s CliffordSimp pass, which lead to non-linear runtime requirement. Because this pass is not applied by the SquashTK1 approach and all other transformations passes described in this paper have a constant per-gate runtime while also iterating a fixed amount of times over each gate, the runtime scaling of the SquashTK1 approach is linear. The standard deviation for the largest 50 circuits it is strictly under 3% of the average runtime.

The impact of different compilation stages on the result is depicted in Fig. 16. As a naive compilation, the gates of the original circuit are substituted by using Pytket’s RebaseCustom pass as described in Sec. 4.4 and the ZZ decomposition given in (9) and (20). Af-

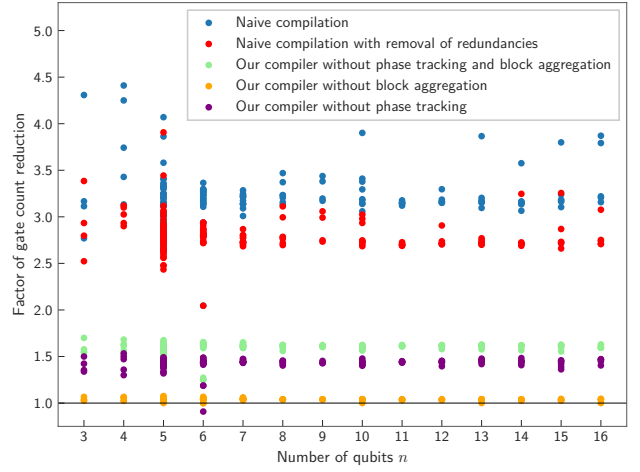


Fig. 16: The factors of the gate count reduction of our complete compilation flow compared to less optimized compilations. For the less optimized compilations the following are used: (1) A naive compilation only substituting the gates with respect to the restricted native gate set  $\mathcal{N}$ , but without any optimization (blue points), (2) the naive compilation with additional removal of trivial redundancies (red points), (3) the compilation as depicted in Fig. 3, but without phase tracking and block aggregation (green points), (4) the compilation only without phase tracking (purple points) and (5) the compilation only without block aggregation (orange points). Where necessary, the compilation result with the better of the two different rebasing approaches is chosen. The circuits are sorted by the number of qubits they operate on. For all circuits which reduction factor is over 1 (the horizontal black line) the complete compilation flow of our compiler produces a circuit with a lower gate count than less optimized compilations.

terwards, the circuit is transformed to the restricted native gate set  $\mathcal{N}$ . When comparing this naive transformation to our compiler, the resulting circuits of our compiler have 2.05 up to 5.38 times less single qubit gates and up to 1.60 times less two-qubit gates. On average our compiler produces the circuits which overall gate count is 3.22 times lower. This naive transformation determines for all evaluated circuits results with a 1.09 times lower gate count when not excluding the Ry from the native gate set before executing the RebaseCustom pass. This is the case because the naive transformation must not take care of commutations and including Ry gates allows to substitute the gates by shorter gate sequences.

When comparing our compiler with the naive approach, but additionally removing trivial redundancies via the Pytket RemoveRedundancies pass, the compiled circuits have between 2.35 and 4.84 times less single qubit gates and up to 1.50 times less two-qubit gates. The overall gate count of our compiler is on average 2.80 times lower than the overall gate count of the improved naive transformation. These high factors show the potential of the optimizations our compiler applies. In the improved naive transformation for 98% of the circuit the result have a lower

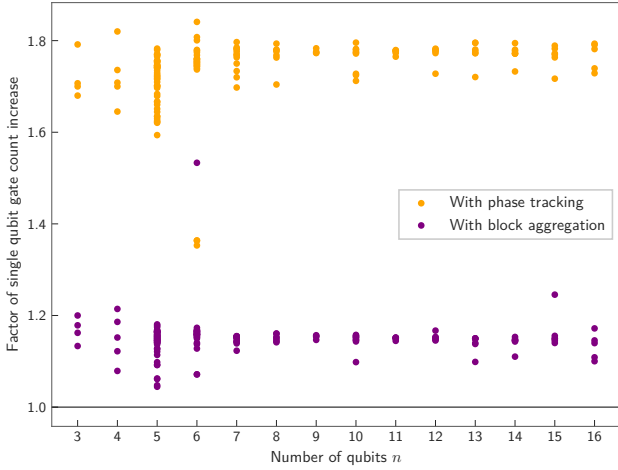


Fig. 17: The factors of the single qubit gate count increase of the compilation as depicted in Fig. 3 without phase tracking and block aggregation compared to the compilation only with phase tracking (orange points) and only with block aggregation (purple points). As compilation results the better of the two different rebasing approaches is chosen. The circuits are sorted by the number of qubits they operate on.

or equal gate count when excluding the Ry gate from the native gate set before executing the `RebaseCustom` pass. The reason for this is that excluding gates from the native gate set reduces the number of different gates. Consequently, it is more likely that gates of the same type are next to each other allowing a better removal of redundancies.

In the next evaluation our compiler is executed as depicted in Fig. 3, but with skipping the phase tracking and block aggregation from Sec. 4.7 and Sec. 4.8, respectively. To compare the gate counts, for each circuit the approach (CliffordSimp or SquashTK1) which produces the lowest overall gate count after executing the whole compilation flow was used in all evaluations. If the CliffordSimp and SquashTK1 approach have the same overall gate count, the result with the lower two-qubit gate count was preferred. When comparing the whole compiler flow with the flow skipping these two optimizations, the complete compiler calculates circuits with an 1.35 up to 1.98 times lower single qubit gate count. Because the phase tracking as well as the block aggregation do not change the two-qubit gates, the two-qubit gate count stays the same. The overall gate count of the whole compiler flow is on average 1.59 times lower than in the case of the reduced compiler.

Going in further details, in the following the phase tracking, but not the block aggregation is executed. In this case the overall gate count of the whole compilation flow is on average only 1.04 times and the single qubit gate count up to 1.11 times lower than the gate counts of the flow not executing block aggregation. The impact of the phase tracking and block aggregation on the single qubit gate count can be seen in Fig. 17. A compilation without phase tracking

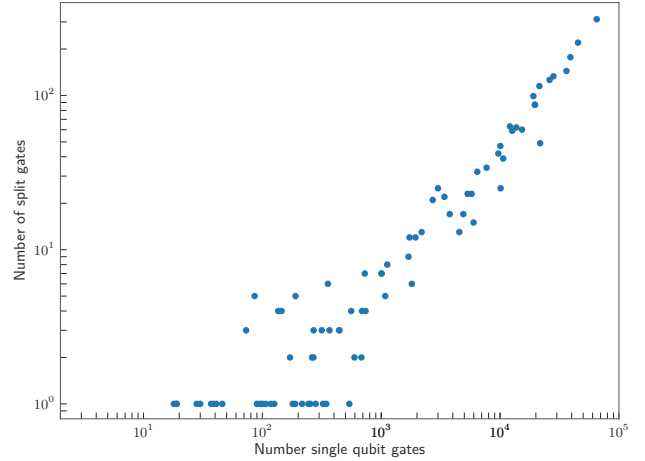


Fig. 18: Number of single qubit gates in the original circuit on which splits are applied during angle splitting from Sec. 4.8.2. Every point represents one circuit of the benchmark on which angle splitting is applied.

and block aggregation has an 1.35 up to 1.84 times higher single qubit gate count than the compilation with phase tracking. This shows that the large part of the improvements, which can be achieved after transforming the single qubit gates to the restricted native gate set  $\mathcal{N}$ , is realized by phase tracking.

In the opposite case, where block aggregation without phase tracking is performed, the overall gate count of the whole compilation flow is on average 1.43 times and the single qubit gate count is between 0.88 and 1.73 times lower than the counts of the flow not applying phase tracking. While in the previous comparisons all circuits have better gate counts when executing our whole compilation flow, here is one circuit, *graycode6\_47*, which has a lower single qubit gate count when phase tracking is not applied. The reason for this is the construction of this circuit consisting only of CNOT gates. Consequently, this circuit directly provokes from the symmetric structure of the CNOT decomposition in (10) favoring block aggregations. Compared to a compilation without phase tracking and block aggregation, a compilation with block aggregation has an 1.04 up to 1.53 times lower gate count. Thus, the impact of block aggregation is lower than the impact of phase tracking. Evaluating the angle splitting from Sec. 4.8.2 shows that this technique is applied to 56% of the circuits. On these circuits angle splitting is applied on 0.19% up to 5.81% and on average on 0.62% of the single qubit gates in the original circuits. The number of single qubit gates of the original circuit which are split by the angle splitting are shown in Fig. 18. This number grows with the number of single qubit gates.

## 5.2 Comparison to other compilers

We benchmark our compiler against built-in Pytket routines, using its `FullPeepholeOptimise` pass,

which is a combination of Pytket’s `CliffordSimp`, `RemoveRedundancies`, `CommuteThroughMultis`, `KAKDecomposition` and `EulerAngleReduction` passes. Then, the circuits are rebased to  $\{\text{Rx}, \text{Rz}, \text{ZZ}\}$  using Pytket’s `RebaseCustom` pass with the TK1 decomposition from (8a) and the CNOT decomposition from (10). After rebasing, the repeated removal and commutation of gates based on Pytket’s built-in procedures from Sec. 4.2 is applied. As Pytket does not allow to restrict the gates of the native gate set to certain angles, it cannot directly transform the gates to the restricted native gate set  $\mathcal{N}$ . To render the gate counts to be comparable, the transformation from Sec. 4.6 is applied to the circuit.

For the Qiskit compilation, first the ZZ decomposition given in (9) and (20) is applied to  $C$  since Qiskit cannot transform ZZ gates with  $\theta \neq \frac{\pi}{2}$  already in  $C$  to ZZ gates with  $\theta = \frac{\pi}{2}$  and a set of single qubit gates. Afterwards, Qiskit’s `BasisTranslator` pass is applied with the target basis  $\{\text{Rx}, \text{Ry}, \text{Rz}, \text{ZZ}\}$ . After rebasing, the `transpile` function of the Qiskit compiler module is executed with optimization level 3. Like Pytket, Qiskit cannot transform the gates to the restricted native gate set  $\mathcal{N}$ , such that we employ Sec. 4.6 to obtain comparable gate counts.

In addition to the standard passes of Pytket and Qiskit, we also benchmark against the Pytket extension `pytket-aqt`. Because this extension was developed for AQT’s ion trap quantum computer, the native gate set supported by this extension is specified for this quantum computer and consists of the set  $\{\text{Rx}, \text{Ry}, \text{XX}\}$ . The circuits were compiled with optimization level 2 provided by the `pytket-aqt` extension using the `sim` device which is an ideal simulator of the AQT quantum device. Although the compiled circuits are in a different native gate set after compilation, the circuits were not transformed to the restricted native gate set  $\mathcal{N}$  in this case. This allows the comparison of the optimization process of two existing ion trap quantum computer architectures.

In comparison with the compiler of AQT, our compiler generates circuits with a lower or equal gate count in 96% of the time. The gate counts of the circuits calculated by our compiler are reduced by a factor from 0.89 up to 1.31 compared to the results of the AQT compiler. For 97% of the circuits our single qubit gate count and for 79% our two-qubit gate count is lower than or equal to AQT’s gate counts. The reduction of the single qubit gate count is given by a factor between 0.85 and 1.45, the two-qubit gate count reduction by a factor from 0.83 up to 1.20. Comparing the resulting circuits reveals that the difference in gates is in large parts due to our block aggregation (see Sec. 4.8). When not applying block aggregation, the overall and single qubit gate counts are only lower or equal in 89% of the cases, while the ranges of the reduction factors do not change. The AQT compiler does not perform such a translation since their archi-

tecture consists of one large ion chain and not several smaller chains stored at different trap segments. This difference in the target architectures and the resulting block aggregation technique seems to be the main reason for the different compilation results. Like our compiler, the AQT compiler reduces the circuits `qft_10` and `qft_16` to empty circuits. The runtime needed by our compiler is reduced by a factor of up to 12.47 compared to the AQT compiler.

Compared to standard Pytket, our compiler can nearly always find a result with lower gate count in a faster time. In numbers, there are between 2.09 and 3.66 times less gates and a runtime reduction of a factor from 1.08 up to 11.18. Like in the comparison with the AQT compiler the circuits `qft_10` and `qft_16` are two exceptions because they can be reduced to empty circuits by our compiler as well as Pytket. A more detailed examination reveals that for all sample circuits our compiler produces results with 2.41 to 4.65 times less single qubit gates, while the two-qubit gate count is only for 81% of the circuits up to 1.33 times less or equal.

The comparison to the Qiskit pass shows that our compilation leads to 1.38 up to 2.21 times fewer final gates, when excluding the circuits `qft_10` and `qft_16`, which Qiskit does not reduce to an empty circuit in contrast to our compiler. Furthermore, when ignoring these two circuits, the single qubit gate count is between 1.55 and 2.41 times fewer for our compilation and the two-qubit gate count between 1.00 and 1.60 times, never being higher than for the Qiskit compilation. Regarding the runtime, for 90% of sample circuits the Qiskit compiler is faster than our compiler by a factor up to 1.68. For the remaining 13 circuits – excluding the circuits `qft_10` and `qft_16` – our compiler is faster by a factor between 1.00 and 1.72. However, Qiskit’s faster runtime is paid by a significantly larger number of gates.

The gate count reduction that can be achieved by our compiler compared to AQT, Pytket and Qiskit is summarized in Fig. 19. The greatest reduction is achieved compared to Pytket with an average reduction factor of 2.75, followed by Qiskit with 1.68 and AQT with 1.08. As mentioned earlier, the latter is mostly due to the different quantum hardware architecture and is reduced to 1.04 when accounting for that effect. In the case of Pytket and Qiskit, our compiler always yields circuits with a lower gate count.

## 6 Conclusion and outlook

We have presented a quantum circuit compiler for a shuttling-based ion trap quantum computer that implements a number of optimization techniques like phase tracking and block aggregation to reduce the number of gates when compiling a quantum circuit into the native gate set.

In comparison with other compilation algorithms, our

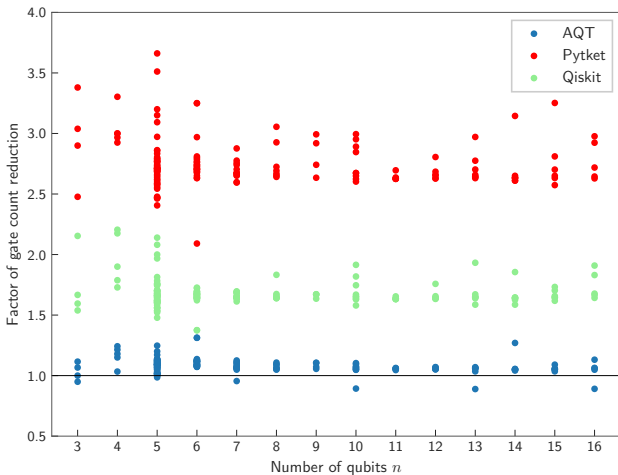


Fig. 19: The factors of the gate count reduction of our compiler compared to AQT, Pytket and Qiskit. As our compilation result, the better of the two different rebasing approaches is chosen. The circuits are sorted by the number of qubits they operate on. For all circuits which reduction factor is over 1 (the horizontal black line) our approach with the lowest gate count produces a circuit with a lower gate count than AQT, Pytket or Qiskit.

compiler reduces the gate count by a factor of up to 1.31 (AQT), up to 3.66 (Pytket) and up to 2.21 (Qiskit). Also the runtime is reduced by a factor of up to 12.47 for AQT and up to 11.18 for Pytket. Qiskit has by a factor up to 1.68 shorter compilation time, but at the expense of a significantly larger number of gates.

In the future we plan to enhance the functionality of the compiler, to increase its performance using more advanced compilation techniques and to adapt it for more powerful architectures. One particular feature is the utilization of parameterized gates, which will allow the compilation of variational circuits such as the variational quantum eigensolver (VQE) [36]. The next architectural step will be the adaption to a platform for allowing simultaneous addressed manipulation of larger subsets of commonly confined trapped-ion qubits, where gates can be carried out in parallel. This will allow for low-resource quantum computation on sub-registers, interleaved with time-consuming register reconfiguration steps. Future multiplexed laser addressing units [37] will also allow for carrying out multi-qubit gates, such that e.g., three-qubit Toffoli gates can be realized within a single laser interaction sequence [38] rather than being decomposed into two-qubit gates. This can massively increase the quantum computational power of a trapped-ion platform, but also calls for an advanced compilation layer.

## 7 Acknowledgements

We acknowledge funding by the Germany ministry of science and education (BMBF) via the VDI within

the projects HFAK and IQuAn. The research is based upon work supported by the Office of the Director of National Intelligence (ODNI), Intelligence Advanced Research Projects Activity (IARPA), via the U.S. Army Research Office grant W911NF-16-1-0070. The views and conclusions contained herein are those of the authors and should not be interpreted as necessarily representing the official policies or endorsements, either expressed or implied, of the ODNI, IARPA, or the U.S. Government. The U.S. Government is authorized to reproduce and distribute reprints for Governmental purposes notwithstanding any copyright annotation thereon. Any opinions, findings, and conclusions or recommendations expressed in this material are those of the author(s) and do not necessarily reflect the view of the U.S. Army Research Office.

## References

- [1] F. Arute et al. “Quantum supremacy using a programmable superconducting processor”. *Nature* **574**, 505–510 (2019).
- [2] L. Postler et al. “Demonstration of fault-tolerant universal quantum gate operations” (2021). [arXiv:2111.12654](https://arxiv.org/abs/2111.12654).
- [3] L. Egan et al. “Fault-tolerant control of an error-corrected qubit”. *Nature* **598**, 281–286 (2021).
- [4] J. Preskill. “Quantum Computing in the NISQ era and beyond”. *Quantum* **2**, 79 (2018). [arXiv:1801.00862v3](https://arxiv.org/abs/1801.00862v3).
- [5] D. Kielpinski, C. Monroe, and D. J. Wineland. “Architecture for a large-scale ion-trap quantum computer”. *Nature* **417**, 709 (2002).
- [6] V. Kaushal et al. “Shuttling-based trapped-ion quantum information processing”. *AVS Quantum Science* **2**, 014101 (2020). [arXiv:1912.04712](https://arxiv.org/abs/1912.04712).
- [7] J. M. Pino et al. “Demonstration of the trapped-ion quantum CCD computer architecture”. *Nature* **592**, 209–213 (2021).
- [8] J. Hilder et al. “Fault-tolerant parity readout on a shuttling-based trapped-ion quantum computer”. *Phys. Rev. X* **12**, 011032 (2022). [arXiv:2107.06368](https://arxiv.org/abs/2107.06368).
- [9] Durandau, J. and Brunet, C. and Poschinger, U. G. and Mailhot, F. and Bérubé-Lauzière, Y. “Automatic shuttling sequence generation for a linear ion trap computer”. *Bulletin of the American Physical Society* (2021). url: [meetings.aps.org/Meeting/MAR21/Session/F34.6](https://meetings.aps.org/Meeting/MAR21/Session/F34.6).
- [10] A. A. Saki, R. O. Topaloglu, and S. Ghosh. “Muzzle the shuttle: Efficient compilation for multi-trap trapped-ion quantum computers”. In

- 2022 Design, Automation & Test in Europe Conference & Exhibition (DATE). Pages 322–327. (2022). [arXiv:2111.07961](#).
- [11] T. Schmale et al. “Backend compiler phases for trapped-ion quantum computers” (2022). [arXiv:2206.00544](#).
- [12] M. Webber, S. Herbert, S. Weidt, and W. K. Hensinger. “Efficient qubit routing for a globally connected trapped ion quantum computer”. *Advanced Quantum Technologies* **3**, 2000027 (2020). [arXiv:2002.12782](#).
- [13] S. Sivarajah et al. “t|ket): a retargetable compiler for NISQ devices”. *Quantum Science and Technology* **6**, 014003 (2020). [arXiv:2003.10611](#).
- [14] V. Bergholm et al. “Pennylane: Automatic differentiation of hybrid quantum-classical computations” (2018). [arXiv:1811.04968](#).
- [15] R. Wille, R. Van Meter, and Y. Naveh. “Ibm’s qiskit tool chain: Working with and developing for real quantum computers”. In 2019 Design, Automation Test in Europe Conference Exhibition (DATE). Pages 1234–1240. (2019).
- [16] E. A. Martinez, T. Monz, D. Nigg, P. Schindler, and R. Blatt. “Compiling quantum algorithms for architectures with multi-qubit gates”. *New J. Phys.* **18**, 063029 (2016). [arXiv:1601.06819](#).
- [17] T. Nguyen et al. “Quantum circuit transformations with a multi-level intermediate representation compiler” (2021). [arXiv:2112.10677](#).
- [18] D. Maslov. “Basic circuit compilation techniques for an ion-trap quantum machine”. *New J. Phys.* **19**, 023035 (2017). [arXiv:1603.07678](#).
- [19] B. Coecke and R. Duncan. “Interacting quantum observables: categorical algebra and diagrammatics”. *New J. Phys.* **13**, 043016 (2011). [arXiv:0906.4725](#).
- [20] X. Zhou, S. Li, and Y. Feng. “Quantum circuit transformation based on simulated annealing and heuristic search”. *IEEE Transactions on Computer-Aided Design of Integrated Circuits and Systems* **39**, 4683–4694 (2020). [arXiv:1908.08853](#).
- [21] A. Zulehner, A. Paler, and R. Wille. “An efficient methodology for mapping quantum circuits to the ibm qx architectures”. *IEEE Transactions on Computer-Aided Design of Integrated Circuits and Systems* **38**, 1226–1236 (2019). [arXiv:1712.04722](#).
- [22] A. Cowtan et al. “On the Qubit Routing Problem”. In 14th Conference on the Theory of Quantum Computation, Communication and Cryptography (TQC 2019). Volume 135 of *Leibniz International Proceedings in Informatics (LIPIcs)*, pages 5:1–5:32. Dagstuhl, Germany (2019). Schloss Dagstuhl–Leibniz-Zentrum fuer Informatik. [arXiv:1902.08091](#).
- [23] G. Li, Y. Ding, and Y. Xie. “Tackling the qubit mapping problem for nisq-era quantum devices”. In Proceedings of the Twenty-Fourth International Conference on Architectural Support for Programming Languages and Operating Systems, ASPLOS. Pages 1001–1014. ACM (2019). [arXiv:1809.02573](#).
- [24] A. Y. Kitaev. “Quantum computations: algorithms and error correction”. *Russian Mathematical Surveys* **52**, 1191–1249 (1997).
- [25] C. M. Dawson and M. A. Nielsen. “The solovay-kitaev algorithm”. *Quantum Information and Computation* **6**, 81–95 (2006). [arXiv:quant-ph/0505030](#).
- [26] A. Sørensen and K. Mølmer. “Quantum computation with ions in thermal motion”. *Phys. Rev. Lett.* **82**, 1971–1974 (1999). [arXiv:quant-ph/9810039](#).
- [27] H. Kaufmann et al. “Fast ion swapping for quantum-information processing”. *Phys. Rev. A* **95**, 052319 (2017). [arXiv:1607.03734](#).
- [28] H. Kaufmann, T. Ruster, C. T. Schmiegelow, F. Schmidt-Kaler, and U. G. Poschinger. “Dynamics and control of fast ion crystal splitting in segmented paul traps”. *New J. Phys.* **16**, 073012 (2014). [arXiv:1403.0097](#).
- [29] M. W. van Mourik et al. “Coherent rotations of qubits within a surface ion-trap quantum computer”. *Phys. Rev. A* **102**, 022611 (2020). [arXiv:2001.02440](#).
- [30] Cambridge Quantum Computing Ltd. “pytket.circuit.OpType — pytket 1.1.0 documentation”. url: [cqcl.github.io/tket/pytket/api/optype.html](https://cqcl.github.io/tket/pytket/api/optype.html). (accessed: 01.06.2022).
- [31] A. Fagan and R. Duncan. “Optimising clifford circuits with quantomatic”. *Electronic Proceedings in Theoretical Computer Science* **287**, 85–105 (2019). [arXiv:1901.10114v1](#).
- [32] D. C. McKay, C. J. Wood, S. Sheldon, J. M. Chow, and J. M. Gambetta. “Efficient  $z$  gates for quantum computing”. *Phys. Rev. A* **96**, 022330 (2017). [arXiv:1612.00858](#).
- [33] Z. Xiangzhen (2019). code: [Ben-sonZhou1991/circuittransform commit:8e6e5b1](#).
- [34] Alpine Quantum Technologies GmbH. “AQT Pytket Tutorial”. url: [www.aqt.eu/aqt-pytket-tutorial](https://www.aqt.eu/aqt-pytket-tutorial). (accessed: 01.06.2022).
- [35] I. Pogorelov et al. “Compact ion-trap quantum computing demonstrator”. *PRX Quantum* **2**, 020343 (2021). [arXiv:2101.11390](#).

[36] J. Tilly et al. “The variational quantum eigensolver: a review of methods and best practices” (2021). [arXiv:2111.05176](#).

[37] I. Pogorelov et al. “Compact ion-trap quantum computing demonstrator”. [PRX Quantum](#)

[2, 020343](#) (2021). [arXiv:2101.11390](#).

[38] Y. Shapira et al. “Theory of robust multiqubit nonadiabatic gates for trapped ions”. [Phys. Rev. A](#) **101**, 032330 (2020). [arXiv:1911.03073](#).

# Appendix

## A Detailed evaluation results

This appendix shows the detailed results of the evaluations described in [Sec. 5.1](#) and [Sec. 5.2](#). The results for the circuits with 3 to 5 qubits are presented in [Tab. 1](#) and the results for the circuits with 6 to 16 qubits in [Tab. 2](#). All 149 quantum circuits are taken from [\[33\]](#).

Tab. 1: Results of the evaluations for the circuits with 3 to 5 qubits. In the first column the name, the number of qubits (q) as well as the number of single qubit and two-qubit gates of the original circuit are displayed. The number of single qubit and two-qubit gates for the original circuit as well as the benchmarks are shortened by 1qg and 2qg, respectively. In the next two columns the single qubit and two-qubit gate counts of our CliffordSimp and SquashTK1 approaches are shown. The last three columns show results of AQT as well as the Pytket and Qiskit standard passes. In each of these columns the first two entries show the single qubit and two-qubit gate counts. The last entry in each column shows the factor the overall gate count is reduced compared to the best approach of our compiler (r\_g).

Original Circuit				Our CliffordSimp approach		Our SquashTK1 approach		AQT			Pytket			Qiskit		
Name	q	1qg	2qg	1qg	2qg	1qg	2qg	1qg	2qg	r_g	1qg	2qg	r_g	1qg	2qg	r_g
ex-1_166	3	10	9	22	8	24	9	24	8	1.07	79	8	2.90	41	9	1.67
ham3_102	3	9	11	19	7	18	9	22	7	1.12	71	8	3.04	45	11	2.15
3_17_13	3	19	17	48	17	48	17	48	17	1.00	144	17	2.48	83	17	1.54
millier_11	3	27	23	60	22	56	23	56	19	0.95	248	19	3.38	103	23	1.59
4gt11_84	4	9	9	22	8	26	9	23	8	1.03	80	9	2.97	48	9	1.90
rd32-v0_66	4	18	16	30	10	29	12	34	12	1.15	105	12	2.93	71	16	2.17
rd32-v1_68	4	20	16	29	10	32	12	34	12	1.18	105	12	3.00	70	16	2.21
decod24-v0_38	4	28	23	46	20	51	21	62	20	1.24	198	20	3.30	95	23	1.79
decod24-v2_43	4	30	22	49	21	56	22	63	22	1.21	188	22	3.00	99	22	1.73
4mod5-v0_20	5	10	10	28	9	30	10	32	10	1.14	91	10	2.73	50	10	1.62
4mod5-v1_22	5	10	11	27	9	36	11	27	9	1.00	96	11	2.97	61	11	2.00
mod5d1_63	5	9	13	31	12	30	13	33	13	1.07	107	13	2.79	56	13	1.60
4gt11_83	5	9	14	32	11	33	14	32	12	1.02	119	14	3.09	64	14	1.81
4gt11_82	5	9	18	31	12	42	18	32	13	1.05	135	16	3.51	74	18	2.14
4mod5-v0_19	5	19	16	42	16	42	16	50	16	1.14	134	16	2.59	81	16	1.67
mod5mils_65	5	19	16	44	16	44	16	51	16	1.12	139	16	2.58	86	16	1.70
4mod5-v1_24	5	20	16	42	16	42	16	48	16	1.10	137	16	2.64	73	16	1.53
alu-v0_27	5	19	17	50	17	50	17	51	17	1.01	148	17	2.46	86	17	1.54
alu-v1_28	5	19	18	50	18	51	18	51	18	1.01	155	18	2.54	88	18	1.56
alu-v1_29	5	20	17	52	17	52	17	51	17	0.99	149	17	2.41	85	17	1.48
alu-v2_33	5	20	17	50	17	50	17	56	17	1.09	149	17	2.48	89	17	1.58
alu-v3_35	5	19	18	51	17	48	18	50	17	1.02	146	17	2.47	85	18	1.56
alu-v4_37	5	19	18	51	17	48	18	50	17	1.02	146	17	2.47	85	18	1.56
alu-v3_34	5	28	24	66	24	66	24	67	24	1.01	206	24	2.56	113	24	1.52
mod5d2_64	5	28	25	65	25	65	25	73	25	1.09	211	25	2.62	121	25	1.62
4gt13_92	5	36	30	74	29	73	30	82	30	1.09	249	30	2.71	141	30	1.66
4gt13-v1_93	5	38	30	75	29	75	30	86	30	1.12	250	30	2.69	140	30	1.63
4mod5-v0_18	5	38	31	65	28	80	31	86	30	1.25	262	31	3.15	152	31	1.97
4mod5-v1_23	5	37	32	77	32	77	32	87	32	1.09	266	32	2.73	144	32	1.61
one-two-three-v2_100	5	37	32	75	30	76	32	91	32	1.17	261	32	2.79	145	32	1.69
one-two-three-v3_101	5	38	32	80	32	80	32	92	32	1.11	272	32	2.71	147	32	1.60
4gt5_75	5	45	38	98	37	100	38	111	38	1.10	315	38	2.61	184	38	1.64
alu-v0_26	5	46	38	98	38	99	38	105	38	1.05	312	38	2.57	180	38	1.60
rd32_270	5	48	36	94	36	96	36	96	34	1.00	326	34	2.77	174	36	1.62
decod24-v1_41	5	47	38	83	37	94	38	107	37	1.20	347	37	3.20	176	38	1.78
4gt5_76	5	45	46	88	36	114	46	98	35	1.07	409	45	3.66	212	46	2.08
4gt13_91	5	54	49	117	45	117	49	130	47	1.09	392	47	2.71	226	49	1.70
4gt13_90	5	54	53	117	46	123	53	130	48	1.09	408	49	2.80	234	53	1.76
alu-v4_36	5	64	51	123	49	123	49	134	48	1.06	419	48	2.72	233	51	1.65
4gt5_77	5	73	58	142	56	144	58	161	58	1.11	473	58	2.68	271	58	1.66
one-two-three-v1_99	5	73	59	138	58	140	59	163	58	1.13	503	58	2.86	270	59	1.68
one-two-three-v0_98	5	81	65	150	61	163	65	174	63	1.12	534	64	2.83	303	65	1.74
4gt10-v1_81	5	82	66	162	64	167	66	177	65	1.07	544	66	2.70	310	66	1.66
decod24-v3_45	5	86	64	162	63	160	64	179	64	1.08	530	64	2.65	297	64	1.61
aj-e11_165	5	82	69	174	69	174	69	183	68	1.03	589	68	2.70	320	69	1.60
4mod7-v0_94	5	90	72	165	69	178	72	192	69	1.12	578	70	2.77	339	72	1.76
alu-v2_32	5	91	72	176	72	176	72	207	72	1.13	594	72	2.69	340	72	1.66
4mod7-v1_96	5	92	72	164	68	173	70	194	69	1.13	574	70	2.78	334	72	1.75
mod10_176	5	100	78	192	77	197	78	200	76	1.03	653	77	2.71	368	78	1.66
4_49_16	5	118	99	222	95	232	97	259	97	1.12	809	97	2.86	440	99	1.70
hwb4_49	5	126	107	247	99	250	105	267	100	1.06	848	102	2.75	482	107	1.70
mod10_171	5	136	108	248	106	261	108	280	107	1.09	870	108	2.76	496	108	1.71
mini-alu_167	5	162	126	303	124	305	126	337	126	1.08	1,011	126	2.66	576	126	1.64
one-two-three-v0_97	5	162	128	318	127	317	128	348	128	1.07	1,029	128	2.60	594	128	1.62
alu-v2_31	5	253	198	464	196	482	198	526	198	1.10	1,578	198	2.69	910	198	1.68

Tab. 2: Continuation of Tab. 1 for the circuits with 6 to 16 qubits.

Original Circuit			Our CliffordSimp approach		Our SquashTK1 approach		AQT			Pytket			Qiskit			
Name	q	1qg	2qg	1qg	2qg	1qg	2qg	1qg	2qg	r_g	1qg	2qg	r_g	1qg	2qg	r_g
graycode6_47	6	0	5	17	5	17	5	20	5	1.14	41	5	2.09	31	5	1.64
ex1_226	6	2	5	11	5	11	5	16	5	1.31	47	5	3.25	17	5	1.38
xor5_254	6	2	5	11	5	11	5	16	5	1.31	47	5	3.25	17	5	1.38
decod24-bdd_294	6	41	32	80	32	79	32	87	32	1.07	277	32	2.78	150	32	1.64
4gt4-v0_80	6	100	79	190	79	198	79	225	79	1.13	658	79	2.74	371	79	1.67
4gt12-v0_88	6	108	86	208	85	211	86	241	86	1.12	700	86	2.68	400	86	1.66
4gt12-v1_89	6	128	100	245	100	245	100	279	100	1.10	828	100	2.69	468	100	1.65
4gt4-v0_79	6	126	105	244	100	244	103	271	102	1.08	828	102	2.70	478	105	1.69
4gt4-v0_78	6	126	109	252	104	254	107	276	106	1.07	870	107	2.74	495	109	1.70
4gt12-v0_87	6	135	112	267	109	274	112	307	112	1.11	905	112	2.70	517	112	1.67
4gt12-v0_86	6	135	116	269	110	279	116	307	113	1.11	921	114	2.73	524	116	1.69
4gt4-v0_72	6	145	113	277	113	277	113	312	113	1.09	913	113	2.63	529	113	1.65
4gt4-v1_74	6	154	119	291	119	291	119	323	118	1.08	969	118	2.65	546	119	1.62
decod24-enable_126	6	189	149	369	148	366	149	408	149	1.08	1,207	149	2.63	694	149	1.64
mod8-10_178	6	190	152	361	152	363	152	422	152	1.12	1,245	152	2.72	697	152	1.65
4gt4-v0_73	6	216	179	416	169	438	179	468	169	1.09	1,439	179	2.77	831	179	1.73
ex3_229	6	228	175	415	174	432	175	484	175	1.12	1,452	175	2.76	809	175	1.67
mod8-10_177	6	244	196	464	191	473	196	522	192	1.09	1,560	193	2.68	892	196	1.66
alu-v2_30	6	281	223	512	219	528	221	600	221	1.12	1,761	221	2.71	1,009	223	1.69
mod5adder_127	6	316	239	552	239	583	239	644	239	1.12	1,984	239	2.81	1,085	239	1.67
sf_276	6	442	336	787	336	806	336	896	336	1.10	2,806	336	2.80	1,547	336	1.68
sf_274	6	445	336	752	336	814	336	891	336	1.13	2,895	336	2.97	1,537	336	1.72
hwb5_53	6	738	598	1,399	590	1,418	598	1,554	593	1.08	4,782	595	2.70	2,673	598	1.64
4mod5-bdd_287	7	39	31	81	31	80	31	77	29	0.95	259	29	2.59	148	31	1.61
alu-bdd_288	7	46	38	94	38	95	38	108	38	1.11	315	38	2.67	179	38	1.64
rd53_135	7	162	134	325	134	325	134	359	134	1.07	1,083	134	2.65	620	134	1.64
ham7_104	7	171	149	346	145	360	149	379	145	1.07	1,214	149	2.78	677	149	1.68
C17_204	7	262	205	503	205	503	205	540	203	1.05	1,689	203	2.67	960	205	1.65
rd53_131	7	269	200	467	197	502	198	549	198	1.13	1,712	198	2.88	926	200	1.70
rd53_133	7	324	256	610	250	622	252	662	249	1.06	2,045	251	2.67	1,199	256	1.69
majority_239	7	345	267	648	266	665	267	707	266	1.06	2,205	266	2.70	1,243	267	1.65
ex2_227	7	356	275	645	275	672	275	749	275	1.11	2,260	275	2.76	1,276	275	1.69
rd53_130	7	595	448	1,074	447	1,120	448	1,218	448	1.01	3,720	448	2.74	2,077	448	1.66
sym6_145	7	2,187	1,701	4,186	1,701	4,186	1,701	4,544	1,701	1.06	13,593	1,701	2.60	7,916	1,701	1.63
hwb6_56	7	3,771	2,952	7,020	2,940	7,069	2,952	7,806	2,948	1.08	23,500	2,949	2.66	13,474	2,952	1.65
rd53_138	8	72	60	135	56	161	60	152	56	1.09	499	60	2.93	290	60	1.83
cm82a_208	8	367	283	699	283	707	283	751	281	1.05	2,363	281	2.69	1,326	283	1.64
f2_232	8	681	525	1,283	525	1,301	525	1,375	525	1.05	4,271	525	2.65	2,444	525	1.64
rd53_251	8	727	564	1,332	563	1,369	564	1,509	563	1.09	4,600	563	2.72	2,608	564	1.67
ur2_277	8	10,046	10,066	20,683	9,595	21,760	10,062	23,839	9,693	1.11	82,522	9,981	3.06	40,267	10,066	1.66
hwb7_59	8	13,698	10,681	25,519	10,643	25,787	10,677	27,907	10,655	1.07	84,861	10,656	2.64	48,855	10,681	1.65
ur2_152	8	45,270	35,210	83,255	34,974	84,418	35,210	90,708	35,030	1.06	280,368	35,030	2.67	158,880	35,210	1.64
con1_216	9	539	415	997	414	1,024	415	1,099	414	1.07	3,454	414	2.74	1,942	415	1.67
ur5_280	9	26,065	23,764	51,470	22,886	54,374	23,742	59,003	23,097	1.10	193,444	23,620	2.92	100,571	23,764	1.67
ur1_278	9	28,074	26,692	56,024	25,606	59,686	26,676	64,488	25,831	1.11	217,795	26,513	2.99	109,607	26,692	1.67
hwb8_113	9	39,008	30,372	73,631	30,304	74,701	30,368	79,432	30,306	1.06	243,495	30,307	2.63	139,611	30,372	1.64
mini_alu_305	10	96	77	195	77	194	77	211	77	1.06	641	77	2.65	351	77	1.58
qft_10	10	110	90	0	0	0	0	0	0	-	0	0	-	49	90	-
sys6-v0_111	10	117	98	226	93	255	98	242	93	1.05	810	98	2.85	459	98	1.75
rd73_140	10	126	104	233	98	273	104	264	98	1.09	853	104	2.89	498	104	1.82
ising_model_10	10	390	90	274	90	274	90	235	90	0.89	1,000	90	2.99	607	90	1.91
rd73_252	10	3,002	2,319	5,606	2,316	5,715	2,319	6,200	2,319	1.08	18,859	2,319	2.67	10,773	2,319	1.65
sqn_258	10	5,764	4,459	10,737	4,455	10,916	4,459	11,804	4,454	1.07	36,153	4,454	2.67	20,617	4,459	1.65
sym9_148	10	12,096	9,408	23,223	9,405	23,134	9,408	24,693	9,408	1.05	75,283	9,408	2.60	43,809	9,408	1.64
max46_240	10	15,282	11,844	29,040	11,839	29,159	11,844	31,340	11,827	1.06	95,430	11,827	2.62	54,782	11,844	1.63
ur3_279	10	64,982	60,380	128,608	58,152	138,302	60,346	147,412	58,646	1.10	491,283	60,036	2.95	251,262	60,380	1.67
wim_266	11	559	427	1,063	427	1,062	427	1,151	427	1.06	3,484	427	2.63	2,003	427	1.63
dc1_220	11	1,081	833	2,050	833	2,059	833	2,182	833	1.05	6,768	833	2.64	3,886	833	1.64
z4_268	11	1,730	1,343	3,248	1,342	3,299	1,343	3,542	1,338	1.06	11,035	1,338	2.70	6,251	1,343	1.65
life_238	11	12,645	9,800	23,953	9,792	24,142	9,800	25,847	9,797	1.06	78,873	9,797	2.63	45,433	9,800	1.64
9symm1_195	11	19,649	15,232	37,316	15,217	37,558	15,232	40,178	15,221	1.05	122,688	15,221	2.63	70,510	15,232	1.63
sym9_193	11	19,649	15,232	37,316	15,217	37,558	15,232	40,178	15,221	1.05	122,688	15,221	2.63	70,510	15,232	1.63
sym9_146	12	180	148	342	141	387	148	376	141	1.07	1,207	148	2.81	701	148	1.76
cm152a_212	12	689	532	1,303	532	1,313	532	1,399	531	1.05	4,348	531	2.66	2,480	532	1.64
sqrt8_260	12	1,695	1,314	3,167	1,313	3,243	1,314	3,468	1,314	1.07	10,712	1,314	2.68	6,104	1,314	1.66
cycle10_2_110	12	3,402	2,648	6,452	2,633	6,454	2,644	6,922	2,638	1.05	21,235	2,638	2.63	12,227	2,648	1.64
rd84_253	12	7,698	5,960	14,507	5,957	14,620	5,960	15,714	5,948	1.06	48,350	5,948	2.65	27,649	5,960	1.64
sym10_262	12	36,199	28,084	68,695	28,069	69,669	28,084	74,122	28,080	1.06	226,402	28,080	2.63	129,977	28,084	1.63
rd53_311	13	151	124	306	124	306	124	322	123	1.03	1,039	123	2.70	558	124	1.59
ising_model_13	13	513	120	366	120	366	120	312	120	0.89	1,324	120	2.97	819	120	1.93
squar5_261	13	1,124	869	2,078	869	2,145	869	2,268	866	1.06	7,312	866	2.78	4,056	869	1.67
radd_250	13	1,808	1,405	3,434	1,405	3,467	1,405	3,736	1,403	1.06	11,372	1,403	2.64	6,564	1,405	1.65
adr4_197	13	1,941	1,498	3,655	1,492	3,705	1,498	4,008	1,497	1.07	12,113	1,497	2.64	7,007	1,498	1.65
root_255	13	9,666	7,493	18,139	7,493	18,337	7,493	19,735	7,487	1.06	60,646	7,487	2.66	34,752	7,493	1.65
dist_223	13	21,422	16,624	40,547	16,622	40,761	16,624	43,742	16,614	1.06	133,794	16,614	2.63	77,068	16,624	1.64
0410184_169	14	107	104	207	97	260	102	285	101	1.27	854	102	3.14	460	104	1.86
sym6_316	14	147	123	307	123	308	123	325	123	1.04	1,000	123	2.61	559	123	1.59